Heterogeneous Dynamics and Mechanisms of Primary Cilium Disassembly in Mammalian Cells

Mary Mirvis[1], Kathleen Siemers[1,2], James Nelson[1,2], Tim Stearns[2,3]

[1]Departments of [1]Molecular and Cellular Physiology, [2]Biology, and [3]Genetics, Stanford University, Stanford, CA, 94305

Corresponding author:
Tim Stearns
Dept. of Biology
Stanford University
Stanford, CA 94305-5020
(650) 725-6934
stearns@stanford.edu

Abstract

The primary cilium is an important regulator of signaling pathways in cell proliferation and differentiation. Mechanisms involved in cilium assembly and homeostasis are well described, but little is known about mammalian ciliary disassembly, which is required for cell cycle progression. We examined whether cilia disassembly in cultured mouse cells occurred by resorption into the cell or extracellular shedding. Live cell imaging of individual disassembly events revealed dynamic and heterogeneous behaviors, with rates varying by several orders of magnitude. Surprisingly, seconds-fast disassembly was the predominant method of cilium loss (83% of events), and we demonstrate that this is due to ciliary shedding. We tested the roles of candidate regulators of ciliary shedding, katanin and intracellular calcium. Katanin overexpression increased seconds-fast disassembly, and katanin and intracellular calcium levels independently, but not synergistically, reduced cilia length. This work provides new, detailed insights into mechanisms of primary ciliary disassembly in mammalian cells.

Introduction

Eukaryotic cilia and flagella are highly conserved organelles adapted to facilitate the interaction of cells with the surrounding environment. Many types of cilia are found in a wide diversity of organisms, tissues and cell types, with variable structural features underlying specific functions. Nevertheless, all cilia and flagella share a common structure consisting of a mature centriole (a basal body in this context), which nucleates a core of stable microtubule doublets (the axoneme), encased in a ciliary membrane distinct in composition from the plasma membrane. Contact between the basal body/axoneme and plasma membrane occurs near the base of the cilium at the transition zone, which is thought to segregate the ciliary compartment from the cytoplasm, thereby maintaining a specific population of proteins in the cilium (1–3).

The primary cilium occurs in single copy per cell in most vertebrate tissues, where it receives and transduces mechanical and molecular signals. In this role, primary cilia are essential for coordinating proliferative, metabolic, and developmental signaling pathways including Hedgehog, Receptor Tyrosine Kinase (RTK) growth factors (PDGF, TGF−β, IGF), GPCRs, and non-canonical Wnt(4–6). Furthermore, the primary cilium itself may contribute to cell cycle regulation (7–10). The importance of normal ciliary function is underscored by the diverse phenotypes associated with ciliopathies, developmental syndromes that occur when ciliary structure, function, or regulation are defective (11–13).

Primary cilia are closely intertwined with the cell cycle. In most proliferating animal cells, the primary cilium forms in G0/G1 and is disassembled prior to M-phase, releasing the centrioles to associate with the mitotic spindle (7,14). Cilium disassembly is linked to cell cycle progression and failure to disassemble the cilium is associated with defects in S-phase (7,15–17) and mitotic progression (18–21). Thus the primary cilium is not only dependent on cell cycle

cues for assembly and disassembly, but also the state of the cilium has direct consequences on cell cycle progression (19,21,22).

Ciliary disassembly typically occurs in S or G2. Several cell cycle-associated regulators of ciliary disassembly have been identified (23–26). Notably, mitotic kinase Aurora A (and its homolog CALK in *Chlamydomonas*) activates a phosphorylation cascade required for ciliary disassembly and mitotic progression (19,21,27–32). A proposed mechanism is that the downstream target of Aurora A, the microtubule deacetylase HDAC6, deacetylates stable microtubules of the axoneme, thus destabilizing the axoneme and preparing it for subsequent disassembly, perhaps involving the IFT machinery or microtubule depolymerizing kinesins (30,33,34). Although there is little evidence for this mechanism in mammalian cells, it is consistent with a mechanism for flagellar disassembly in the unicellular green alga *Chlamydomonas*, in which cells gradually and simultaneously resorb their two flagella, defined as internalization of the axoneme and retention of the majority of the ciliary membrane (28,29,35–38).

Alternatively, cilia could be removed very rapidly by extracellular shedding, defined as concurrent release of membrane and axoneme from the cell body, which has also been referred to as ciliary excision, deciliation, deflagellation, or flagellar autotomy (39,40). Ciliary shedding has been observed in several ciliated protozoan species, particularly *Chlamydomonas* (40). Mammalian primary cilia have been observed to undergo pharmacologically-induced shedding (41), and release of a small distal portion of the primary ciliary membrane has been reported in several contexts (42–44), but the relevance of either of these events to whole cilium loss is unknown.

Here, we examined ciliary disassembly dynamics in mouse IMCD3 (inner medullary collecting duct) cells by high resolution, live-cell 3D confocal microscopy. Ciliary disassembly behaviors were remarkably dynamic and heterogeneous, and occurred on time scales ranging from seconds to hours, which we separated into 3 categories (*gradual*, *instant*, and *combined*) of which the fastest (10^1 μm/min; *instant*) comprised >80% of events and involved cilium shedding. We showed that katanin and intracellular calcium, two candidate regulators of ciliary shedding, independently, but not synergistically, negatively regulated cilia disassembly.

Results

Ciliary structures in cells undergoing serum-induced cilium disassembly

We manipulated serum level in mammalian cell culture medium to synchronize the presence of primary cilia in IMCD3 cells (21,45) expressing a fluorescent ciliary membrane marker (IMCD3-SSTR3::GFP) (46). The axoneme in these cells was visualized by immunostaining for acetylated tubulin (acTub), and the basal body by staining for pericentrin (PCNT) (Fig. 1A, S1A). We found that 60 +/- 9.09% of serum starved cells at 0 hour and 6 hours were ciliated after serum starvation. Re-introduction of serum (serum stimulation) over a 6 hour period resulted in a steady loss of cilia to a level of 30 +/- 0.4% that was similar to that in asynchronously cycling cells at a comparable cell density (Fig. 1B). There was also a decrease in mean ciliary length (Fig. S1C). As validation of serum-induced ciliary disassembly, cells were treated in parallel with 2 μM tubacin an inhibitor of HDAC6, a microtubule deacetylase required for ciliary disassembly (21,47,48), or the carrier DMSO as a control. As expected, tubacin treatment prevented the decrease in the percent of ciliated cells (Fig. 1B) and cilia length (Fig. S1C). Mitotic cells (identified by condensed nuclei mitotic spindles, separating nuclei in telophase, and cells separated by a midbody) accumulated following serum stimulation (Fig. Sl); this is consistent with an inverse relationship between the

presence of a primary cilium and the mitotic status (49–51). As expected, this wave of mitosis was inhibited or delayed in tubacin-treated cells (Fig. S1B).

We identified three types of cilium structures consistent with being disassembly intermediates in these fixed samples (Fig. 1C-G): 1) a discontinuous axoneme, marked by a gap in acTub staining ("Discontinuous acTub", Fig. 1C); 2) a ciliary stub, characterized by a short (<1μm) cilium positive for both acTub and SSTR3 membrane fluorescence ("acTub+ SSTR3+ Stub", Fig. 1D); and 3) an axoneme lacking SSTR3 fluorescence, marked by linear acTub fluorescence (>1μm) adjacent to a PCNT-labeled basal body ("acTub+ SSTR3-", Fig. 1E). These structures were rare in serum starved cells, but at 2-3 hrs post-stimulation they comprised the majority of detectable cilia (Fig. 1F). The enrichment of these structures in post-serum stimulated cells was inhibited in the presence of tubacin (Fig. 1G), indicating that these structures are most likely representative of disassembling cilia.

The precise disassembly mechanisms represented by these different structures cannot be determined from static images; however, they illustrate that ciliary disassembly may be unexpectedly complex, and several distinct disassembly behaviors may occur within a single cell type.

Ciliary disassembly dynamics are heterogeneous and favor instantaneous cilia loss

To observe cilium disassembly directly, we generated IMCD3 cells stably co-expressing markers of the ciliary membrane (SSTR3-GFP) and basal body (mCherry-PACT). Live cells were imaged immediately following serum stimulation with full confocal stacks acquired continuously at 45-90 sec intervals for 6-12 hours on a laser scanning confocal microscope. Imaging of cilia in serum starved cells with cilia that were not disassembling (Fig. 2A.1) revealed several intrinsic features

of ciliary dynamics. First, cilia underwent spontaneous length fluctuations on short-term time scales (up to ~1.5 μm between consecutive time points; Fig. S3A). Second, cilium length on average decreased slightly over the 12 hour imaging period, with a mean rate of ~0.005 μm/min (n=10, Fig. S3A), which may reflect individual cell behavior or response to our long-term fluorescence imaging regime. These features were taken into account in our analysis of cilium disassembly.

Video sequences of cells in which cilia disassembled during the course of observation, revealed a striking dynamic range of disassembly behaviors. Further analysis showed that these behaviors can be grouped into three categories, which we will refer to as *gradual*, *instant*, and *combined*; these are illustrated in the individual examples shown in Fig. 2A and Movies S1-4. We define these categories as follows: *gradual* - cilium length reduction over multiple consecutive time points ultimately leading to terminal cilium loss (e.g., Fig. 2A.2, rate of 0.016 μm/min); *instant* - a single discrete event of cilium loss within a single imaging frame, i.e. 30-90 sec (e.g., Fig. 2A.3, approximate minimum rate of 4.72 μm/min); and *combined* – a period of *gradual* disassembly directly followed by an *instant* loss event (e.g., Fig. 2A.4, gradual phase with a rate of 0.029 μm/min, followed by very rapid loss within 46 sec with an approximate minimum rate of 5.69 μm/min). We note that it was usually not possible to visualize the nature of the loss event in the *instant* cases due to their rapid rate and constraints on the time resolution of long time-scale live imaging.

Our initial characterization of the cilium disassembly categories relied on visual inspection of video sequences (Fig S2). To achieve a more objective analysis of disassembly, we developed a Matlab algorithm that normalized ciliary length fluctuations of individual cilia to controls, reliably identified a disassembly start point, and assigned each disassembly behavior to one of the

three categories above, defined in the algorithm as follows: *gradual* if ciliary length just before complete disassembly ($L_{final-1}$) was reduced compared to the length at the start of disassembly (L_{start}); *instant* if $L_{final-1}$ was greater than 1.5 μm, below which length measurements were unreliable due to possible measurement error (Fig. S3A); *combined* if criteria for both *gradual* and *instant* were met in the same ciliary disassembly event (Fig. S3B, Materials & Methods).

To assess overall ciliary behaviors of each category, disassembly curves were normalized by time (normalized to 1000 arbitrary units) and ciliary length (normalized to the maximum length of each cilium), and averaged (Fig. 2C-E). The averaged curve of the *gradual* category shows early, initial ciliary shortening with event start points (circles) distributed along the curve, followed by a period of consistent length reduction in the last ~150 normalized time units as the slope of the curve increased (Fig. 2C). The averaged curve of the *instant* category appears nearly horizontal until the last point, when the curve drops precipitously in a single time point; disassembly start points were nearly all clustered in the last ~10 time units (Fig. 2D). The averaged curve of the *combined* category was intermediate between the *gradual* and *instant* plots, with a slight downward slope of gradual dynamics followed by a rapid loss of cilia length, with start points distributed along the curve (Fig. 2E).

The resulting disassembly rates from our Matlab analysis were in the range of 10^{-3} – 10^{1} μm/min (Fig. 2F). The fastest rate was for *instant* disassembly and was in the range of 10^{1} μm/min. For the *combined* category, separate disassembly rates were calculated from the *gradual* and *instant* stages of cilia loss. Interestingly, the rate of the first *gradual* step of *combined* disassembly (0.083 μm/min ± 0.259) was not significantly different from that of the *gradual*-only rate (0.079 μm/min ± 0.106), and the second (*instant*) step (3.414 μm/min ± 2.098) was comparable to the *instant*-only rate (3.882 μm/min ± 1.802) (Fig. 2F). However, the majority of ciliary length in the

176 *combined* category (72.6 ± 4.5%) was lost during the *instant* stage. These results indicate that the
177 *combined* disassembly behavior likely represents both *gradual* and *instant* mechanisms within the
178 same cilium, rather than a separate mechanism accounting for the biphasic dynamics.

179 Finally, we asked whether there was a correlation between the initiation of ciliary
180 disassembly after serum stimulation and disassembly behavior. Disassembly start and end times
181 were plotted as a histogram (Fig. S4). *Gradual* disassembly events most frequently initiated in the
182 first two hours of serum stimulation (Fig. S4A), although the sample size was low due to the
183 relative rarity of this event (n=11). *Instant* disassembly events increased progressively over the
184 first three hours of stimulation, and appeared to be more widely distributed throughout the time
185 course (Fig. S4B). Interestingly, *combined* category disassembly start times, marking the onset of
186 the initial *gradual* stage, were most frequent in the first two hours after stimulation. *Combined* end
187 points, which occurred with *instant* dynamics, progressively increased over the first three hours,
188 in agreement with the *instant* category (Fig. S4C). These results further illustrate that *combined*
189 disassembly behaviors share features of *gradual* and *instant* disassembly behaviors.

190 Taken together, our analysis identified three categories for primary cilia disassembly
191 behavior in IMCD3 cells: *gradual*, *instant*, and *combined*. Importantly, the *instant* and *combined*
192 categories jointly account for 83.1% (n=70) of all ciliary disassembly events (Fig. 2G), and the
193 *instant* step in the *combined* category accounted for approximately 75% of ciliary length loss.
194
195 **_Instant_ cilia loss dynamics are consistent with extracellular shedding**
196 Our results show that in mammalian cells the final stages of cilia disassembly and loss are on the
197 time scale of seconds, which is several orders of magnitude more rapid than expected for
198 resorption mechanisms as reported in *Chlamydomonas.* However, much more rapid cilium

retraction into the cell has been reported in other unicellular eukaryotes, such as the chytrid fungi (52). To better determine the mechanism of cilium disassembly in mammalian cells we sought to identify sequences in which the loss event could be visualized.

In a rare instance, we observed direct shedding of ciliary membrane from the cell surface (Fig. 3A, Movie S5). In addition, ciliary shedding induced by treatment with dibucaine had similar qualitative features and dynamic profiles to serum-induced *instant* disassembly (Fig. S5) (40,41,53). The rapid nature of complete ciliary detachment in under 54 secs, and the diffusion of the shed remnant(s) away from the site of origin is consistent with our observations of the disappearance of the ciliary membrane with *instant* dynamics in 83.1% of disassembly events (Fig. 2G).

The shed cilia in Fig. 3A have a fragmented appearance. We interpret this as being the result of the free ciliary fragment moving at a faster rate than the rate of z-stack acquisition, rather than sequential loss of small segments of the cilium. Because the shed cilium travels some distance in the time between individual z-slice acquisitions, the apparent location of an object in that slice will have shifted. As a result, the final imaged object appears distorted – artificially elongated or with the appearance of separated fragments. We note that the membrane segments in such sequences were usually visualized as a group that moved together, rather than dispersing independently, consistent with the interpretation that they are all part of the same structure imaged at different times.

We asked whether the cilium was released with or without the axoneme. Excision of portions of the ciliary membrane alone has been previously reported (42–44). To test this, IMCD3-SSTR3::GFP cells were transiently transfected with mCherry-α-tubulin, stimulated with serum, and imaged at 30 sec intervals. Tubulin was observed in shed ciliary fragments (Fig. 3B, Movie

S8), suggesting that the axoneme is shed together with the ciliary membrane and distinguishing this event from previously described ciliary membrane-fragment or ectosome release (42–44).

Validation of ciliary shedding by isolation of ciliary fragments from culture media

Observation of discrete shedding of the entire visible ciliary membrane supported the hypothesis that this behavior underlies *instant* ciliary disassembly dynamics (Fig 3A). Given the limitations of imaging described above, it was important to demonstrate the form in which the cilium is shed. We sought to detect ciliary fragments in the culture medium, predicted to be present based on the hypothesis of shedding as the mechanistic basis for *instant* disassembly.

Previously described methods of cilia isolation from mammalian cells have required artificial deciliation to synchronously release sufficient amounts of ciliary material for detection (41,54). To detect ciliary fragments released spontaneously from serum-stimulated cells we developed two novel methods (Fig. 3). First, immune-capture of cilia allowed direct visualization of the size and shape of unperturbed, shed ciliary fragments. In brief, culture medium from serum-stimulated cells was incubated on glass-bottomed imaging dishes coated with an antibody specific for the extracellular N-terminus of SSTR3 (Fig. S6A). Cilia expressing SSTR3-GFP bound the antibody (Fig. S6B), and were imaged, unfixed, by fluorescence (Fig. 3C) or after fixation, by electron microscopy (Fig 3E). A representative image of an antibody-captured, intact cilium is shown from IMCD3-SSTR3::GFP cells transfected with mCherry-α-tubulin to mark the axoneme (Fig. 3C). The jagged appearance of cilia in these samples is due to thermal motion in surrounding aqueous solution during stack acquisition. Quantification showed a 4-fold increase in cilia captured from medium from serum-stimulated cells compared to control medium from serum-starved cells.

As expected, pre-treating serum-stimulated cells with tubacin resulted in a decrease in the amount of captured cilia to levels in the control (Fig. 3D).

However, the cilia immune-capture method was limited by low amounts of material and instability of antibody-bound cilia, which made analysis by immunofluorescence or biochemistry difficult. Therefore, we developed a filter-spin cilia isolation method to concentrate large volumes of medium containing ciliary fragments (Fig. 3F&G, S6B). 40-80 mL of serum-starved or -stimulated culture media were subjected to a combination of filtration and centrifugation steps to concentrate ciliary material approximately 500-fold. As a positive control, serum-starved cells were scraped and treated with high-calcium deciliation buffer (55) to induce artificial shedding of cilia (see *Materials and Methods*). Immunostaining for ciliary markers (IFT88 and α-tubulin) demonstrated increased abundance of ciliary structures in the concentrated material, many with the dimensions expected of shed primary cilia (Fig. 3F). Western blotting for IFT88, α-tubulin, and acetylated tubulin further confirmed detectable levels of cilia-specific proteins in the concentrated medium (Fig. 3G).

Together, immune-capture and filter-spin concentration methods for ciliary isolation demonstrated the presence and correct dimensions of intact cilia containing ciliary membrane (SSTR3), axonemal tubulin, and other specific ciliary markers that were shed from serum-stimulated cells. The consistent detection of full-length, tubulin-containing cilia by two independent methods indicates that ciliary shedding is a physiological behavior of IMCD3 cells, and is a likely explanation for the most prevalent, *instant* ciliary disassembly behavior.

p60 katanin activity regulates ciliary disassembly behaviors

We next examined the roles of potential regulators of ciliary shedding in the disassembly behaviors that we had observed. In *Chlamydomonas,* the deflagellation-incompetent mutant Fa1p carries a mutation in a gene homologous to katanin, a conserved microtubule-severing AAA ATPase with roles in mitotic spindle formation and function, and axon extension in mammalian cells (56–58). In *Chlamydomonas*, katanin directly triggers axoneme severing *in vitro* and localizes to the site of axoneme breakage at the transition zone (39,59,60). Katanin overexpression also induced ciliary disassembly in *Tetrahymena* (61).

In order to determine whether katanin activity contributed to ciliary disassembly by shedding in mammalian cells, we overexpressed the catalytic domain of mouse katanin, p60 (KATNA1) in IMCD3-SSTR3::GFP cells. We imaged tRFP fluorescence for the transfected p60, and used a p60-specific antibody for total katanin (including endogenous protein) in IMCD3-SSTR3::GFP-turboRFP(tRFP) control and IMCD3-SSTR3::GFP-tRFP::p60 cells. Both endogenous p60 and tRFP-p60, but not tRFP alone, were located at mitotic spindles and diffusely in the cytoplasm. In some cells, a punctum of katanin fluorescence was clearly detected at the basal body of cilia (Fig. 4A). The level of cytoplasmic acetylated tubulin was reduced significantly in serum-starved and -stimulated (2 hr) tRFP-p60 expressing cells compared to the control (Fig. S6A-B), indicating that over-expressed katanin was active and induced increased severing and destabilization of cytoplasmic microtubules (61,62).

We assessed the effect of p60 overexpression on ciliary abundance, length, and disassembly behavior on a population level. Fixed, serum-starved tRFP- and tRFP-p60-expressing cells displayed similar levels of ciliation and responded similarly to 6-hour serum stimulation (Fig. S6C). However, ciliary length was significantly reduced in tRFP-p60 cells, as measured from confocal z-stacks of live cells (Fig. 4B). Tubacin and cytochalasin D treatments

289 inhibited ciliary disassembly in both tRFP and tRFP-p60 cells (Fig. S6D). These results indicate
290 that p60 activity did not impair overall ciliogenesis or spontaneously induce ciliary disassembly,
291 but reduced ciliary length.
292 Next, we asked whether tRFP-p60 overexpression affected ciliary disassembly dynamics.
293 Ciliary disassembly events were observed and analyzed as described above (see Fig. 2). In tRFP
294 expressing cells, *combined* disassembly was the largest category of disassembly events (53.3%,
295 n=61). In tRFP-p60 cells, *gradual* disassembly was virtually eliminated, while the frequency of
296 *instant* disassembly increased ~33% (n=50). Cumulative average disassembly curves normalized
297 to disassembly time and cilium length further illustrated a difference in ciliary disassembly
298 dynamics (Fig. 4D-G). Due to the low frequency of *gradual* disassembly events, only *combined*
299 and *instant* behaviors are discussed further. In both *combined* and *instant* disassembly categories,
300 the cumulative curves from tRFP expressing control cells (Fig. 4D&F) have a steeper slope than
301 the equivalent plots from p60 overexpressing cells (Fig. 4E&G). These data demonstrate that in
302 tRFP-p60 cells ciliary disassembly by *gradual* dynamics (either *gradual*-alone or *combined*
303 events) was generally reduced, and *instant* disassembly was more prevalent.
304
305 ***Intracellular calcium does not act synergistically with p60 to promote ciliary shedding***
306 High extracellular calcium and drug-induced increases in intracellular calcium levels have been
307 used to artificially force ciliary shedding in ciliates, flagellates, and mammalian cells
308 (40,41,55,63). However, mechanisms underlying this effect have not been elucidated. Calcium-
309 calmodulin signaling is upstream of AurA, a key activator of ciliary disassembly (20), indicating
310 a role for changes in cytoplasmic calcium levels in ciliary disassembly. We tested whether or not

311 increased intracellular calcium levels and katanin worked synergistically to promote ciliary
312 shedding.

313 To examine the roles of intracellular calcium levels and p60 overexpression in cilia
314 disassembly, we used well-known small molecule modulators of intracellular calcium levels
315 (dibucaine (40,41,64,65), ionomycin (66), and thapsigargin (41,67) increase cytoplasmic calcium
316 levels; BAPTA-AM, a calcium chelating agent, reduces calcium levels (68)) on tRFP- and tRFP-
317 p60-overexpressing IMCD3 cells, and ciliation rates and length were quantified (Fig. 5).

318 tRFP and tRFP-p60 expressing cells were serum-starved, pre-treated with dibucaine,
319 ionomycin or thapsigargin, fixed, and the percentage of cells that were ciliated was measured.
320 Cilia counts for each treatment were normalized to levels in DMSO-treated cells to give a
321 relative change in ciliation. Both dibucaine and ionomycin caused a significant reduction in the
322 abundance and length of cilia in both tRFP- and tRFP-p60-expresssing cells (Fig. 5AB). These
323 results indicate that increased cytoplasmic calcium levels, either through release of intracellular
324 membrane-bound calcium (dibucaine, (64,65)) or influx of extracellular calcium (ionomycin,
325 (66)), had similar effects in negatively regulating primary cilia, and that tRFP-p60
326 overexpression did not affect this response. In contrast, 5 μM thapsigargin, which releases
327 intracellular calcium stores (67,69), reduced ciliary abundance but not length in tRFP expressing
328 cells, and increased the abundance and length of cilia in tRFP-p60 expressing cells (Fig. 5CD).

329 To reduce the level of cytoplasmic calcium, serum-starved cells were pre-treated with
330 BAPTA-AM for 30 min. Consistent with previously published results (20), the percent of
331 ciliated cells after 2 hr and 6 hr serum stimulation was reduced in BAPTA- but not DMSO-
332 treated tRFP expressing cells, demonstrating that ciliary disassembly was inhibited by
333 intracellular calcium chelation. In contrast, tRFP-p60 expressing cells had levels of ciliary

disassembly that were similar in DMSO and BAPTA-AM treated conditions (Fig. 5E). In addition, BAPTA-AM treatment caused a significant reduction in overall ciliary length in tRFP-p60, but not in tRFP expressing cells (Fig. 5F). Taken together, these results indicate that intracellular calcium and katanin do not synergistically promote ciliary loss. The negative relationship between intracellular calcium levels and cilia disassembly may be dependent on the source or concentration of intracellular calcium, and p60 overexpression alters this relationship.

Discussion

We examined cilium disassembly in mammalian cells, using live-cell single-cilium analysis, revealing highly heterogeneous rates of cilium loss, spanning approximately three orders of magnitude, from hours to seconds. These behaviors fell into three categories – *gradual* disassembly (10^{-3} – 10^{-1} μm/min), *instant* disassembly (10^{1} μm/min), and *combined* disassembly, consisting of consecutive *gradual* and *instant* dynamic phases. We conclude from these observations that there may be different mechanisms by which a cilium is disassembled within a single cell type, and even within a single cilium (in the case of *combined* disassembly). We propose that *gradual* disassembly is explained by disassembly of the axoneme and ciliary resorption, and *instant* disassembly is best explained by ciliary shedding. Interestingly, the shedding and resorption behaviors described in *Chlamydomonas*, chytrid fungi, and other organisms, are conserved in very distantly-related mammalian cells.

The co-existence of resorption and shedding in *combined* disassembly is intriguing, as it indicates differential regulation of the distal and proximal portions of the cilium leading to different methods of disassembly in each. A similar phenomenon has been described in *Chlamydomonas*, in which the initial resorption of the bulk of the flagellum was followed by severing the remainder from the basal body and release of a small particle into the surrounding

358 medium (36). The wide range of disassembly rates in the *gradual* category that we observed in
359 IMCD3 cells indicates that there are several resorption mechanisms, or one mechanism with
360 highly tunable dynamics. Thus, a *combined* resorption-severing behavior may be conserved
361 between *Chlamydomonas* and mammalian cells.

362 What could contribute to differential regulation of distal and proximal portions of the
363 cilium? One study showed that that different kinases and downstream effectors control the
364 disassembly of the distal and proximal regions of the flagellum, but both contribute to resorption
365 (29). It is also becoming apparent that structural features of the axoneme may contribute to the
366 regulation of different regions of the cilium, such as the transition from doublet to singlet
367 microtubules or the distribution of microtubule post-translational modifications that are non-
368 uniformly distributed in the axoneme (70–72). Additionally, there may be a length- or time-
369 dependent switch or signal that activates a new mechanism once the cilium has been partially
370 disassembled. The conditions and factors underlying the decision to undergo one type of
371 disassembly over another are likely complex and will require further study.

372 Taking *instant* and *combined* disassembly categories together (because the last stage of
373 *combined* disassembly is an *instant* loss event), *instant* dynamics accounted for the majority of
374 the ciliary disassembly events observed in IMCD3 mammalian cells. Direct observation of
375 tubulin and the membrane marker SSTR3 during ciliary loss from the cell surface indicated
376 extracellular shedding of cilia. This was further supported with two independent methods that
377 isolated ciliary fragments shed into the medium. The presence of ciliary material in serum
378 starvation media was unexpected, but repeatable, and due to two major causes – 1) ciliary
379 shedding is a means for ciliary disassembly, but does not exclusively occur in disassembling
380 cilia, as we have observed shedding and immediate ciliary regrowth in serum starved cells (data

not shown), and 2) cilia yields from the filter-spin concentration method are not reliably quantitative due to the potential for sample loss at several steps.

Regardless of these caveats, the morphology and composition of captured cilia confirmed 3 major points regarding mechanisms of ciliary shedding: 1) cilia are shed as intact structures; 2) the fragmented appearance of shed cilia in live cell imaging are likely the result of confocal imaging of a highly dynamic process, rather than cilium fragmentation; and 3) shed cilia contain tubulin, implying that the axoneme is severed and shed along with the ciliary membrane. These results are also consistent with the observation of discontinuous axonemes, and the frequent observation of *instant* disassembly in which the entire ciliary membrane is shed cleanly from the basal body in response to serum stimulation or dibucaine. Together, these observations strongly support the hypothesis that highly prevalent *instant* disassembly is due to ciliary shedding, and distinguishes our results from previous studies that described the release of ectosomes, apical abscission, and decapitation of the ciliary membrane alone (42–44).

A limitation of our live cell imaging of ciliary disassembly was the high fluorescence background in the cytoplasm, which meant that we could not follow the fate of the axoneme and membrane during ciliary resorption. Nevertheless, in fixed cells we identified several novel non-canonical ciliary structures in serum-stimulated cells that might be ciliary disassembly intermediates, which might provide insight into mechanisms for ciliary shedding and resorption, for example: 1) discontinuous acetylated tubulin staining indicates a break in the axoneme, and the accompanying constriction at that site in SSTR3 membrane fluorescence indicates membrane pinching that could portend ciliary severing at that site prior to shedding; 2) a ciliary stub positive for acetylated tubulin and SSTR3-GFP could represent a remnant of a shed or resorbed cilium close to the cell surface (73), although at this resolution it cannot be determined whether

the ciliary stub is on the cell surface or in the cytoplasm; and, 3) acetylated tubulin fluorescence without corresponding SSTR3 membrane fluorescence indicates a resorbed axoneme-basal body complex in the cytoplasm, as has been observed previously (74), in which the membrane was released or incorporated into the plasma membrane. While these interpretations are speculative, due to the nature of static representations of a dynamic process and the markers of ciliary structures, the relative lack of these ciliary structures in starved and tubacin-treated conditions indicates that they may be representative of the ciliary disassembly process.

We assessed the roles of the microtubule severing enzyme katanin and intracellular calcium in regulating ciliary shedding. Katanin mediates axoneme severing and ciliary shedding in *Chlamydomonas* and *Tetrahymena* (39,60,61,75), and high intracellular calcium levels trigger ciliary shedding in *Chlamydomonas* and mammalian cells (39–41). Overexpression of the katanin catalytic domain p60 reduced ciliary length, and nearly eliminated the *gradual* category of ciliary disassembly, which was compensated for by an increase in the *instant* disassembly category. Therefore, upregulation of katanin activity would likely promote *instant* ciliary disassembly behavior, and, by extension, ciliary shedding. Interestingly, we did not find that p60 overexpression affected general ciliation, in contrast to previous work showing a ciliogenesis defect in response to overexpression of the related proteins katanin-like 2 (KATNAL2) (76) and fidgetin-like 1 (FIGL1) (77). This may be due to differences in protein functions or levels of protein expression, or criteria for categorizing short versus absent cilia. Alternatively, p60-overexpression in serum-starved cells may cause ciliary severing at sites other than the ciliary base (Fig. 1C, 3B), or shedding from the base might be rapidly followed by cilium regrowth in quiescent cells (M. Mirvis, unpublished results), either of which could result in an apparent decrease in the average cilium length in a cell population.

Based on previous work in *Chlamydomonas* showing that both katanin and raised intracellular calcium levels spontaneously induce ciliary breakage and severing *in vivo* and *in vitro* (39), we tested whether they act synergistically in promoting ciliary shedding and overall disassembly in IMCD3 cells. Consistent with previously published results, we found that addition of drugs that raise intracellular calcium levels reduced ciliary number and length, while chelating intracellular calcium inhibited ciliary disassembly in control cells (20,41). Unexpectedly, overexpression of p60 had opposing effects – addition of thapsigargin increased the number and length of cilia, while BAPTA-AM shortened cilia and failed to inhibit serum-induced ciliary loss. Thus, intracellular calcium levels and katanin do not act synergistically or additively to promote ciliary shedding. Little is known regarding a direct relationship between calcium and katanin, although one study showed that p60 has several calcium binding sites, and that calcium binding inhibited p60 severing activity (78). Interestingly, high calcium levels have been shown to affect induce primary cilium bending by altering axoneme microtubule morphology (79).

Our work raises many new questions regarding the mechanisms and dynamics of primary ciliary disassembly that will need to be addressed in future studies. Why do multiple mechanisms for ciliary disassembly exist? Could ciliary resorption and shedding have specific advantages for cell cycle regulation or signaling? How is the ciliary membrane separated from the cell during ciliary shedding? Recently published work identified an actin-dependent phosphoinositide-based pathway underlying ciliary decapitation (43), and ciliary disassembly activator Aurora A may act upstream of this pathway (45). Future work may focus on whether the same mechanism is responsible for membrane detachment at the ciliary base. What is the precise mechanism of axoneme severing by katanin? Future studies using immunogold electron microscopy could

450 determine whether katanin is localized specifically to the transition zone in mammalian cells, as
451 shown in *Chlamydomonas* (59). Furthermore, answering how katanin carries out complete,
452 localized, coordinated disruption of the axoneme despite the complex microtubule structure of
453 the axoneme may provide novel insights into general mechanisms for microtubule severing.
454

455 **Acknowledgements**

456 We thank Jonathan Indig for critical assistance with developing and writing the Matlab
457 algorithm, Fan Ye and the Max Nachury lab for the gift of IMCD3-SSTR3::GFP cells, Martijn
458 Gloerich for assistance with lentivirus, Daniel Cohen and Caitlin Collins for technical assistance
459 with cilia immune-capture, Lydia Joubert and the Beckman Cell Sciences Imaging Facility for
460 assistance with SEM sample preparation and imaging. We thank Jessica Feldman, Lucy O'Brien,
461 Jackson Liang, and members of the Nelson and Stearns laboratories for invaluable discussion of
462 the methods and results. Research reported in this publication was supported by the National
463 Institute of General Medical Sciences of the National Institutes of Health under award number
464 T32GM007276 (M.M.)., R35 GM118064 to W.J.N. and R01GM121424 to T.S. The content is
465 solely the responsibility of the authors and does not necessarily represent the official view of the
466 National Institutes of Health.
467
468
469
470
471
472

Materials & Methods

Cell Culture. IMCD3 cells were grown in DMEM-F12 medium with 10% fetal bovine serum and 1% penicillin-streptomycin-kanamycin antibiotic cocktail. Cells were passaged every 2-3 days at 1:10-1:20 dilution. Cells were tested for mycoplasma with Sigma LookOut Mycoplasma PCR Detection Kit (Cat#MP0035) as directed by the manufacturer, and incidences of mycoplasma contamination was treated with Mycoplasma Removal Agent (MP Biomedicals, #093050044). Following decontamination, experiments potentially affected were repeated at least three times to determine any difference in results. No significant differences were observed.

Serum Starvation and Stimulation. Cells were seeded in 24- or 6-well dishes with glass coverslips for imaging following fixation, or 35 mm glass-bottomed MatTek dishes (#P35G-0-10-C) for live imaging. 24-well dishes were seeded at $1.5x10^4$ cells and 6-well and 35 mm MatTek dishes were seeded at $1\text{-}1.5x10^5$, to achieve 50-70% confluence next day. For serum-starvation, cells were washed once with 0.2% DMEM-F12 + PSK, then grown in 0.2% DMEM-F12 + PSK for 24 hr. Serum stimulation was by either re-addition of FBS directly to dishes to 10% final concentration, or replacement with 10% FBS DMEM-F12.

Antibodies. The following antibodies and dilutions were used. Acetylated tubulin mouse monoclonal 6-11B-1 (1:1000 for IF & WB) (Sigma-Aldrich Cat# T7451); Pericentrin rabbit polyclonal Poly19237 (1:500 for IF) (Covance Cat #PRB-432C, now BioLegend); Arl13b rabbit polyclonal (1:250-1:500 for IF) (Proteintech Cat# 17711-1-AP); N19-SSTR3 antibody (rabbit polyclonal) (Santa Cruz Cat #sc-11610, discontinued); IFT88 rabbit (1:500 for IF & WB) (GeneTex, Cat#79169); α-tubulin YL1/2 (1:1000 for IF & WB), (ThermoFisher #MA1-080017); alpha-tubulin DM1a (1:1000 for IF & WB) (ThermoFisher #62204); rabbit monoclonal anti-p60

EPR5071, (1:250 IF), (Abcam Cat# ab111881); rabbit polyclonal anti-KATNA1, (1:100-250 IF) (Proteintech Cat#17560-1-AP). Anti-rabbit GFP (1:250) (Life Technologies, #A11122); Anti-mouse GFP (1:1000) (Roche, #11063100). Secondary antibodies used were: Anti-mouse Rhodamine (1:1000) (Jackson ImmunoResearch, #715-295-150), Anti-rabbit FITC (1:1000) (Jackson ImmunoResearch, #111-095-003), Anti-rabbit Alexa647 (1:200) (Life Technologies, #A21245), Anti-mouse Alexa647 (1:200) (Life Technologies, #A21236), Hoescht (1:1000-2000) (Molecular Probes, #H-3570).

Chemicals. Tubacin (Sigma-Aldrich, #SML0065) at 2 µM in DMSO; dibucaine hydrochloride, (Sigma-Aldrich #285552) at 190 µM in DMSO. The following were used at 1µM in DMSO: Cytochalasin D (#PHZ1063), Thapsigargin, (Sigma-Aldrich #T9033). BAPTA-AM (Sigma-Aldrich #A1076). Ionomycin 10 mM stock was a gift from the Lewis laboratory, Stanford Univ.

Generation of stable cell lines. IMCD3-SSTR3::GFP-mCherry::PACT: mCherry::PACT was cloned from a pLV plasmid (pTS3488, created by multi-site Gateway cloning by Christian Hoerner) onto pLV-Puro-EF1a construct using Gibson cloning. Lentivirus with the cloned construct was generated in HEK293T and used to infect IMCD3-SSTR3::GFP (gift from Nachury laboratory, (46)) under selection with 800 mg/mL puromycin for 4-5 days. Infected cells were FACS-sorted into polyclonal populations by mCherry fluorescence intensity, and a pool of low-expressing cells were selected to prevent over-expression phenotypes of a centrosomal protein.

Katanin expression constructs: Mammalian expression constructs for turboRFP and turboRFP::p60 (p60 domain of mouse katanin) were designed and ordered from VectorBuilder. All constructs were amplified by transformation in DH5α and maxi-prep (Qiagen #12165).

IMCD3-SSTR3::GFP cells were transfected with each construct with ThermoFisher Lipofectamine 3000 according to manufacturer's protocol (#L3000015). The next day, cells were subjected to G418 selection (800ng/µL for 5-6 days). Cells were sorted by FACS into low-, medium-, and high-expressing pools, and maintained in DMEM-F12 10% FBS + PSK and 250 ng/µL G418 to maintain transgene expression.

Transient transfection. mCherry-α-tubulin mammalian expression construct was a gift from Angela Barth, Stanford Univ., and transfected into IMCD3-SSTR3::GFP cells. Transfections were performed using Lipofectamine 3000 transfection reagent according to manufacturer's protocol.

Immunofluorescence microscopy. Generally, fixation for immunofluorescence microscopy was done with 100% methanol for 5 minutes at -20ºC, followed by washes with 0.1% Triton X-100 in PBS at room temperature for 2 minutes, and 3 PBS washes. Samples were blocked for 1 hr at RTºC or overnight at 4ºC in 2% BSA, 1% goat serum, 75mM NaN_3. Antibodies were diluted to indicated concentrations in blocking buffer. Primary antibody incubations were performed for 1 hr at RTºC or overnight at 4ºC. Secondary antibody incubations were performed for 1-2 hr at RTºC. Following each antibody incubation, samples were washed 3 times in PBS + 0.05% Tween-20 for 5 mins each at RTºC.

Images were acquired with a Zeiss Axiovert 200 inverted epifluorescence microscope and a 63x objective, or a Leica SP8 scanning laser confocal microscope with LASX Software, using mercury or argon lamps with white light laser excitation, and a 63x 1.4 NA oil objective. Exposure times were constant during each experiment. For imaging of serum-starved and serum-stimulated cells, fields of view were selected based on DAPI staining by two critieria: 1) to select

for moderate cell density, in order to avoid effects of high density on cell cycle and ciliation; and 2) to eliminate bias in % cilia quantifications from scanning by ciliary markers.

Live-cell confocal microscopy. Cells were cultured in glass-bottomed Mattek dishes and imaged in DMEM-F12 media with 15mM HEPES without phenol red. Movies were acquired 4-12 hr after serum stimulation with a Leica SP8 scanning laser confocal microscope using 0.5 μm z-slices, 30-90 sec intervals, autofocus, in a 37°C incubator, and red and green channels were acquired simultaneously. The video file was saved as .lif from LASX software and opened in Imaris x64 8.0.2 as a 3D render for analysis of cilia disassembly dynamics and basal body positioning.

Data analysis. Cilia counts and length measurements were performed either manually in Fiji or Imaris x64 8.0.2 and 9.2.1, or through semi-automated detection in Imaris. Manual analysis involved detecting ciliary membrane, marked by an enrichment of SSTR3::GFP above background threshold, that were adjacent to a centriole (mCherry::PACT in dual-fluorescent cells or pericentrin immunofluorescence in single- (SSTR3::GFP-expressing) or non-fluorescent cells), to distinguish from accumulations of SSTR3+ membrane elsewhere in the cell. Manual length measurements in Fiji were made with the line function, and in Imaris with the Measurement tool. Generally, single z-plane images were analyzed in Fiji or Imaris, while confocal z-stacks were analyzed in Imaris which allowed more accurate length measurement due to the 3D render (Surpass) capability. When possible, length measurements in confocal images were semi-automated in Imaris using the Surfaces function to create an artificial object encompassing the ciliary membrane, and exporting Bounding Box data as a proxy for length (the longest dimension of the object).

For live cell serum stimulation experiments, movies were visually scanned in Imaris for examples of disassembling cilia. Images of each disassembling cilium were cropped by time (from t0 to several mins after complete loss), and position (restricted to area of occupancy during the that time window), and then saved in a separate file. To generate ciliary length curves, the ciliary membrane was isolated as an artificial object using the Surface function. When possible, the object was automatically tracked over consecutive time points with length data generated at each time point. In cases where automatic tracking was not possible due to low signal-to-noise of ciliary membrane fluorescence, measurements were taken manually at 15-30 minute intervals until the initiation of ciliary disassembly, and at each time point during the disassembly event.

Matlab: Raw length measurement data from disassembling cilia movies were compiled in to an Excel spreadsheet. A Matlab algorithm imported the data, performed smoothing and calculations of cilium start point, and generated an output file containing disassembly rates, start and end time, start and end length, and proportion length lost per disassembly stage. Algorithm strategy is described in the text and Supplement.

Cilia Isolation. Cell culture: clones of IMCD3 cells, either an unsorted stably expressing GFP-SSTR3 or FACS sorted for medium expression of GFP-SSTR3, were grown on 15cm dishes at $3x10^6$ cells/dish in DMEM/F12 with 10% FBS and antibiotics for 24 hours. The cells were washed 3x with HDF wash buffer, and media was replaced with DMEM/F12 and 0.2% FBS and antibiotics (serum-starved) for 24 hours. Then all dishes were washed 3x with HDF buffer and half received phenol-red free DMEM/F12 with 0.2% FBS (serum-starved), and the other half received phenol red free DMEM/F12 with 10% FBS (serum-stimulated) for 24 hours. Total serum starved time was 48 hours and total serum stimulated time was 24 hours.

584 *Immune-capture Method.* Preparation of antibody-immobilized imaging dishes: Glass in 35 mm
585 glass-bottomed imaging dishes (MatTek) was functionalized by plasma cleaning at 250 moor,
586 Low setting, 45-60 seconds. Dishes were silanized with 500 µL of 2.5% triethoxysilyl-undecanal
587 (TESU) in 100% ethanol, covered with Parafilm and incubated at RT°C for 1hr. Dishes were
588 washed 3x with 100% ethanol, then baked at 85°C for 3 hrs. Next, silanized dishes were treated
589 with the following series of reagents for 1hr at RT°C unless stated otherwise, with 3 PBS washes
590 in between steps: 1) 50mM NHS-LC- LC-biotin in water, 2) 5mg/ml neutravidin for 1hr at
591 RT°C, 3) 300 µg/ml biotin-Protein A 4) block with 15mM D-biotin in DMSO for 30 min, 5) anti-
592 rabbit SSTR3 N19 (extracellular N-terminus) antibody (100-200 µg/mL) at 37°C, followed by
593 one PBS wash. These protocols adapted from Dr. Nicholas Borghi (80).

594 Sample preparation: Culture medium was collected and subjected to centrifugation for 10 min at
595 1000xg at 4°C to remove large cell debris. Samples were then kept on ice until plating on treated
596 dishes or stored at 4°C for a maximum of 1 day. 4mL serum-stimulated or -starved medium was
597 incubated on a treated MatTek dish overnight at 4°C, followed by 3 gentle PBS washes. Samples
598 were then imaged directly, without fixation with a Leica SP8 confocal microscope.

599 SEM: Antibody-immobilized MatTek dishes incubated with serum stimulation medium were
600 fixed for SEM in 4% PFA, 2% glutaraldehyde, and 0.1M Na cacodylate. Glass bottoms were
601 removed, processed for imaging, and imaged with a Hitachi S-3400N VP SEM scope in the
602 Beckman Imaging Facility, Stanford Univ.

603 *Filter-Spin Concentration Method.* Harvest of Cilia: Deciliation of starved IMCD3 cells
604 (positive control): Serum-stimulated or -starved culture medium, or fresh culture medium (with
605 10% FBS, an additional control) was removed from 6 150cm dishes, combined and centrifuged

606 at 200xg at 4°C for 5 mins in the A-4-81 rotor, Eppendorf 5810R centrifuge. Cells were washed
607 2x with warm PBS containing 0.4% EDTA. 10 mL was added to a MatTek dish and incubated
608 for 10 min at 37 °C, followed by gentle up and down pipetting to remove cells from dish. An
609 aliquot of cell suspension was removed for cell count. Cells were centrifuged at 13000 x g for 5
610 mins at RT°C. The cell pellet was resuspended in 5 mL ice cold deciliation buffer (55) (112 mM
611 NaCl, 3.4 mM KCl,10 mM $CaCl_2$, 2.4 mM $NaHcO_3$, 2 mM HEPES, pH7.0 and a protease
612 inhibitor tablet [Roche]). The cell suspension was incubated at 4 °C for 15 mins with rigorous
613 end-over-end rotation, and then centrifuged at 1000 x g for 5 mins at 4 °C in an Eppendorf
614 centrifuge. The resulting supernatant was used for biochemistry and immunostaining.

615 Biochemistry: Half of the supernatant material from deciliated, serum starved or -stimulated cells
616 was centrifuged at 21,000xg for 15 min in JA25.5 rotor in Beckman Coulter Avanti J-25I
617 centrifuge at 4°C. The supernatant was carefully removed, and pellets were resuspended in 160
618 µl of sample buffer (1% SDS, 10mM Tris-HCl, pH 7.5, 2mM EDTA). Samples were boiled at
619 95°C for 8 mins, and equal volumes were separated by 10% PAGE and transferred to PVDF.
620 Blots were blocked (2% BSA, 1% normal donkey and goat serum in TBS, pH 7.4) for 1hr at
621 RT°C or overnight at 4°C. Membranes were blotted with YL1/2 (1:1000), mouse acetylated-
622 tubulin antibody (1:1000), and IFT88 rabbit antibody (1:500) in blocking buffer for 1 hr at
623 RT°C. Blots were washed 5x with TBST. Secondary anti-rabbit, anti-mouse, or anti-rat
624 antibodies labeled with either Alexa Fluor 680 (InVitrogen, #A21058) or IRDye800CW (Li-Cor
625 Biosciences, #926-32213), at 1:30,000 dilution were incubated with blots for 30 min at RT. Blots
626 were washed 5x with TBST and scanned on Licor Odyssey scanner (Li-Cor BioSciences).

627 Immunofluorescence: Half of the supernatant material from deciliated, serum-starved, or -starved
628 and -stimulated cells was concentrated using a 250ml 0.2µm PES filter unit with house vacuum

to reduce the volume to 2 mL, and finally a Millipore Ultrafree-MC filters (PVDF 0.2µm size #UFC30GV100) to reduce the volume to ~0.5 mL. 5 µl of concentrated supernatant was pipetted onto an acid-treated glass slide. A 22 mm acid-treated circular glass coverslip was placed on the sample, and the slide was immediately plunged into liquid nitrogen for ~5 sec. After removing the slide, the coverslip was removed and fixed in -20 °C 100% methanol for 5 mins. Immunofluorescence staining was performed as described above.

Statistics. All analyses were performed in GraphPad Prism. Statistical tests used for each analysis are indicated in the Figure legends. No explicit power analysis was used to determine sample size. All experiments were performed with at least three biological replicates, i.e. samples from independent cell culture passages. When used, technical replicates (i.e. repeats from the same cell culture passage) were averaged for each biological replicate. In brief, comparisons of mean values such as mean percent cilia across replicate experiments were compared using an unpaired t-test. Analyses of individual measurements such as cilia length were subjected to normality tests (Kolmogorov-Smirnoff, D'Agostino & Pearson, and Shapiro-Wilk). If data passed all normality tests, unpaired t-test was used, if not the Mann-Whitney U test was used. If data passed normality by some tests but not others, both types of analyses were performed. Results were similar between parametric and nonparamentric tests.

650 **References**

651 1. Mirvis M, Stearns T, James Nelson W. Cilium structure, assembly, and disassembly
652 regulated by the cytoskeleton. Biochem J. 2018;475(14):2329–53.
653 2. Fisch C, Dupuis-Williams P. Ultrastructure of cilia and flagella - back to the future! Biol
654 Cell. 2011;103(6):249–70.
655 3. Avasthi P, Marshall WF. Stages of ciliogenesis and regulation of ciliary length.
656 2009;49(18):1841–50.
657 4. Mourão A, Christensen ST, Lorentzen E. The intraflagellar transport machinery in ciliary
658 signaling. Curr Opin Struct Biol. 2016;41:98–108.
659 5. Scholey JM, Anderson K V. Intraflagellar Transport and Cilium-Based Signaling. Cell.
660 2006;125(3):439–42.
661 6. Praetorius HA. The primary cilium as sensor of fluid flow: new building blocks to the
662 model. A Review in the Theme: Cell Signaling: Proteins, Pathways and Mechanisms. Am
663 J Physiol - Cell Physiol. 2015;308(3):C198–208.
664 7. Tucker RW, Pardee AB, Fujiwara K. Centriole ciliation is related to quiescence and DNA
665 synthesis in 3T3 cells. Cell. 1979;17(3):527–35.
666 8. Plotnikova O V, Pugacheva EN, Golemis EA. Primary cilia and the cell cycle. Methods
667 Cell Biol. 2009;94(08):137–60.
668 9. Kim S, Tsiokas L. Cilia and cell cycle re-entry: More than a coincidence. Cell Cycle.
669 2011;10(16):2683–90.
670 10. Sung C-H, Li A. Ciliary resorption modulates G1 length and cell cycle progression. Cell
671 Cycle. 2011;10(17):2825–6.
672 11. Plotnikova O V., Golemis EA, Pugacheva EN. Cell cycle-dependent ciliogenesis and

673 cancer. Cancer Res. 2008;68(7):2058–61.

674 12. Hildebrandt F, Benzig T, Katsanis N. Ciliopathies. N Engl J Med. 2016;27(5):743–51.

675 13. Lee K, Battini L, Gusella GL. Cilium, centrosome, and cell cycle regulation in polycystic

676 kidney disease. Biochim Biophys Acta - Mol Cell Res. 2012;1812(10):1263–71.

677 14. Seeley ES, Nachury M V. The perennial organelle: assembly and disassembly of the

678 primary cilium. J Cell Sci. 2010;123(4):511–8.

679 15. Li A, Saito M, Chuang JZ, Tseng YY, Dedesma C, Tomizawa K, Kaitsuka T, Sung C-H..

680 Ciliary transition zone activation of phosphorylated Tctex-1 controls ciliary resorption, S-

681 phase entry and fate of neural progenitors. Nat Cell Biol. 2011;13(4):402–11.

682 16. Kim S, Lee K, Choi JH, Ringstad N, Dynlacht BD. Nek2 activation of Kif24 ensures

683 cilium disassembly during the cell cycle. Nat Commun. 2015;6:1–13.

684 17. Goto H, Inoko A, Inagaki M. Cell cycle progression by the repression of primary cilia

685 formation in proliferating cells. Cell Mol Life Sci. 2013;70(20):3893–905.

686 18. Urrego D, Sánchez A, Tomczak AP, Pardo LA. The electric fence to cell-cycle

687 progression: Do local changes in membrane potential facilitate disassembly of the primary

688 cilium?: Timely and localized expression of a potassium channel may set the conditions

689 that allow retraction of the primary cilium. BioEssays. 2017;39(6):1–6.

690 19. Korobeynikov V, Deneka AY, Golemis EA. Mechanisms for nonmitotic activation of

691 Aurora-A at cilia. Biochem Soc Trans. 2017;45(1):37–49.

692 20. Plotnikova O V., Nikonova AS, Loskutov Y V., Kozyulina PY, Pugacheva EN, Golemis

693 EA. Calmodulin activation of Aurora-A kinase (AURKA) is required during ciliary

694 disassembly and in mitosis. Mol Biol Cell. 2012;23(14):2658–70.

695 21. Pugacheva EN, Jablonski SA, Hartman TR, Henske EP, Golemis EA. HEF1-dependent

Aurora A activation induces disassembly of the primary cilium. Cell. 2007;129(7):1351–63.

22. Sánchez I, Dynlacht BD. Cilium assembly and disassembly. Nat Cell Biol. 2016;18(7):711–7.

23. Wang L, Gu L, Meng D, Wu Q, Deng H, Pan J. Comparative proteomics reveals timely transport into cilia of regulators or effectors as a mechanism underlying ciliary disassembly. J Proteome Res. 2017;16(7):2410–8.

24. Wang W, Wu T, Kirschner MW. The master cell cycle regulator APC-Cdc20 regulates ciliary length and disassembly of the primary cilium. Elife. 2014;3:e03083.

25. Liang Y, Meng D, Zhu B, Pan J. Mechanism of ciliary disassembly. Cell Mol Life Sci. 2016;73(9):1787–802.

26. Lee KH, Johmura Y, Yu LR, Park JE, Gao Y, Bang JK, Zhou M, Veenstra TD, Kim BY, Lee KS. Identification of a novel Wnt5a-CK1ε-Dvl2-Plk1-mediated primary cilia disassembly pathway. EMBO J. 2012;31(14):3104–17.

27. Ran J, Yang Y, Li D, Liu M, Zhou J. Deacetylation of α-tubulin and cortactin is required for HDAC6 to trigger ciliary disassembly. Sci Rep. 2015;5:1–13.

28. Pan J, Wang Q, Snell WJ. An aurora kinase is essential for flagellar disassembly in Chlamydomonas. Dev Cell. 2004;6(3):445–51.

29. Hu Z, Liang Y, He W, Pan J. Cilia disassembly with two distinct phases of regulation. Cell Rep. 2015;10(11):1803–10.

30. Jang C-Y, Coppinger JA, Seki A, Yates JR, Fang G. Plk1 and Aurora A regulate the depolymerase activity and the cellular localization of Kif2a. J Cell Sci. 2009;122(9):1334–41.

719 31. Xu J, Li H, Wang B, Xu Y, Yang J, Zhang X, Harten SK, Shukla D, Maxwell PH, Pei D,
720 Esteban MA. VHL Inactivation Induces HEF1 and Aurora Kinase A. J Am Soc Nephrol.
721 2010;21(12):2041–6.
722 32. Wang G, Chen Q, Zhang X, Zhang B, Zhuo X, Liu J, Jiang Q, Zhang C.. PCM1 recruits
723 Plk1 to the pericentriolar matrix to promote primary cilia disassembly before mitotic
724 entry. J Cell Sci. 2013;126(6):1355–65.
725 33. Cao M, Li G, Pan J. Regulation of cilia assembly, disassembly, and length by protein
726 phosphorylation.. First edit. Vol. 94, Methods in cell biology. Elsevier; 2009. 333-346 p.
727 34. Piao T, Luo M, Wang L, Guo Y, Li D, Li P, Snell WJ, Pan J. A microtubule
728 depolymerizing kinesin functions during both flagellar disassembly and flagellar assembly
729 in Chlamydomonas. Proc Natl Acad Sci U S A. 2009;106(12):4713–8.
730 35. Marshall WF, Rosenbaum JL. Intraflagellar transport balances continuous turnover of
731 outer doublet microtubules: Implications for flagellar length control. J Cell Biol.
732 2001;155(3):405–14.
733 36. Parker JDK, Hilton LK, Diener DR, Rasi MQ, Mahjoub MR, Rosenbaum JL, Quarmby
734 LM. Centrioles are freed from cilia by severing prior to mitosis. Cytoskeleton.
735 2010;67(7):425–30.
736 37. Lefebvre PA, Nordstrom SA, Moulder JE, Rosenbaum JL. ELONGATION AND
737 SHORTENING IN CHLAMYDOMONAS IV. Effects of Flagellar Detachment,
738 Regeneration, and Resorption on the Induction of Flagellar Protein Synthesis. Cell.
739 1978;(36).
740 38. Bloodgood R. Resorption of Organelles Containing Microtubules. Cytobios.
741 1974;9(35):143–61.

742 39. Lohret TA, McNally FJ, Quarmby LM. A role for katanin-mediated axonemal severing
743 during Chlamydomonas deflagellation. Mol Biol Cell. 1998;9(5):1195–207.
744 40. Quarmby LM. Cellular Deflagellation. Int Rev Cytol. 2004;233:47–91.
745 41. Overgaard C, Sanzone K, Spiczka K, Sheff D, Sandra A, Yeaman C. Deciliation is
746 associated with dramatic remodeling of epithelial cell junctions and surface domains. Mol
747 Biol Cell. 2009;20(January):102–13.
748 42. Nager AR, Goldstein JS, Herranz-Pérez V, Portran D, Ye F, Garcia-Verdugo JM, Nachury
749 MV. An actin network dispatches ciliary GPCRs into extracellular vesicles to modulate
750 signaling. Cell. 2017;168(1–2):252–263.e14.
751 43. Phua SC, Chiba S, Suzuki M, Su E, Roberson EC, Pusapati G V., Setou M, Rohatgi R,
752 Reiter JF, Ikegami K, Inoue T. Dynamic remodeling of membrane composition drives cell
753 cycle through primary cilia excision. Cell. 2017;168(1–2):264–279.e15.
754 44. Das RM, Storey KG. Apical abscission alters cell polarity and dismantles the primary
755 cilium during neurogenesis. Science. 2014;343(6167):200–4.
756 45. Plotnikova O V., Seo S, Cottle DL, Conduit S, Hakim S, Dyson JM, Mitchell CA, Smyth
757 IM. INPP5E interacts with AURKA, linking phosphoinositide signaling to primary cilium
758 stability. J Cell Sci. 2015;128(2):364–72.
759 46. Ye F, Nager AR, Nachury M V. BBSome trains remove activated GPCRs from cilia by
760 enabling passage through the transition zone. J Cell Biol. 2018;180620.
761 47. Haggarty SJ, Koeller KM, Wong JC, Grozinger CM, Schreiber SL. Domain-selective
762 small-molecule inhibitor of histone deacetylase 6 (HDAC6)-mediated tubulin
763 deacetylation. Proc Natl Acad Sci. 2003;100(8):4389–94.
764 48. Tran DA-A, Marmo TP, Salam AA, Che S, Finkelstein E, Kabarriti R, Xenias HS,

765 Mazitschek R, Hubbert C, Kawaguchi Y, Sheetz MP, Yao T-P, Bulinski JC. HDAC6
766 deacetylation of tubulin modulates dynamics of cellular adhesions. J Cell Sci. 2007;120(Pt
767 8):1469–79.
768 49. Quarmby LM, Parker JDK. Cilia and the cell cycle? J Cell Biol. 2005;169(5):707–10.
769 50. Ke YN, Yang WX. Primary cilium: An elaborate structure that blocks cell division? Gene.
770 2014;547(2):175–85.
771 51. WHEATLEY D. Expression of Primary Cilia in Mammalian Cells. Cell Biol Int.
772 1996;20(1):73–81.
773 52. Fritz-Laylin LK, Lord SJ, Mullins RD. WASP and SCAR are evolutionarily conserved in
774 actin-filled pseudopod-based motility. J Cell Biol. 2017;216(6):1673–88.
775 53. Satir B, Sale WS, Satir P. Membrane renewal after dibucaine deciliation of Tetrahymena.
776 Freeze-fracture technique, cilia, membrane structure. Exp Cell Res. 1976;97(1):83–91.
777 54. Ishikawa H, Thompson J, Yates JR, Marshall WF. Proteomic analysis of mammalian
778 primary cilia. Curr Biol. 2012;22(5):414–9.
779 55. Raychowdhury MK, McLaughlin M, Ramos AJ, Montalbetti N, Bouley R, Ausiello DA,
780 Cantiello HF. Characterization of Single Channel Currents from Primary Cilia of Renal
781 Epithelial Cells. J Biol Chem. 2005;280(41):34718–22.
782 56. Finst RJ, Kim PJ, Griffis ER, Quarmby LM. Fa1p is a 171 kDa protein essential for
783 axonemal microtubule severing in Chlamydomonas. J Cell Sci. 2000;113 (Pt 1:1963–71.
784 57. Sharp DJ, Ross JL. Microtubule-severing enzymes at the cutting edge. J Cell Sci.
785 2012;125(11):2561–9.
786 58. Matsuo M, Shimodaira T, Kasama T, Hata Y, Echigo A, Okabe M, Arai K, Makino Y,
787 Niwa S-I, Saya H, Kishimoto T. Katanin p60 contributes to microtubule instability around

the midbody and facilitates cytokinesis in rat cells. PLoS One. 2013;8(11):1–15.

59. Lohret TA, Zhao L, Quarmby LM. Cloning of Chlamydomonas p60 katanin and localization to the site of outer doublet severing during deflagellation. Cell Motil Cytoskeleton. 1999;43(3):221–31.

60. Rasi MQ, Parker JDK, Feldman JL, Marshall WF, Quarmby LM. Katanin knockdown supports a role for microtubule severing in release of basal bodies before mitosis in Chlamydomonas. Mol Biol Cell. 2009;20(January):379–88.

61. Sharma N, Bryant J, Wloga D, Donaldson R, Davis RC, Jerka-Dziadosz M, Gaertig J. Katanin regulates dynamics of microtubules and biogenesis of motile cilia. J Cell Biol. 2007;178(6):1065–79.

62. Sudo H, Baas PW. Acetylation of microtubules influences their sensitivity to severing by katanin in neurons and fibroblasts. J Neurosci. 2010;30(21):7215–26.

63. Ishikawa H, Marshall WF. Isolation of mammalian primary cilia. 1st ed. Vol. 525, Methods in Enzymology. Elsevier Inc.; 2013. 311-325 p.

64. Low PS, Lloyd DH, Stein TM, Rogers JAI. Calcium displacement by local anesthetics. J Biol Chem. 1979;254(10):4119–25.

65. Kurebe M. Interaction of dibucaine and calcium ion on a calcium pump reconstituted from defined components of intestinal brush border. Mol Pharmacol. 1977;14:138–44.

66. Liu C, Hermann TE. Characterization of ionomycin as a calcium ionophore. J Biol Chem. 1978;253(17):5892–4.

67. Jones KT, Sharpe GR. Thapsigargin raises intracellular free calcium levels in human keratinocytes and inhibits the coordinated expression of differentiation markers. Vol. 210, Experimental Cell Research. 1994. p. 71–6.

811 68. Tymianski M, Spigelman I, Zhang L, Carlen PL, Tator CH. Mechanism of action and
812 persistence of neuroprotection by Ca2+ chelators. J Cereb Blood Flow Metab.
813 1994;14:911–23.
814 69. Lytton J, Westlin M, Hanley MR. Thapsigargin inhibits the sarcoplasmic or endoplasmic
815 reticulum Ca-ATPase family of calcium pumps. J Biol Chem. 1991;266(26):17067–71.
816 70. Gadadhar S, Dadi H, Bodakuntla S, Schnitzler A, Bièche I, Rusconi F, Janke C. Tubulin
817 glycylation controls primary cilia length. J Cell Biol. 2017;216(9):2701–13.
818 71. O'Hagan R, Silva M, Nguyen KCQ, Zhang W, Bellotti S, Ramadan YH, Hall DH, Barr
819 MM. Glutamylation regulates transport, specializes function, and sculpts the structure of
820 cilia. Curr Biol. 2017;27(22):3430–3441.e6.
821 72. Wloga D, Joachimiak E, Louka P, Gaertig J. Posttranslational modifications of tubulin and
822 cilia. Cold Spring Harb Perspect Biol. 2016;9(6).
823 73. Paridaen JTML, Wilsch-Bräuninger M, Huttner WB. XAsymmetric inheritance of
824 centrosome-associated primary cilium membrane directs ciliogenesis after cell division.
825 Cell. 2013;155(2):333–44.
826 74. Rieder CL, Jensen CG, Jensen LCW. The resorption of primary cilia during mitosis in a
827 vertebrate (PtK1) cell line. J Ultrasructure Res. 1979;68(2):173–85.
828 75. Waclawek E, Joachimiak E, Hall MH, Fabczak H, Wloga D. Regulation of katanin
829 activity in the ciliate Tetrahymena thermophila. Mol Microbiol. 2017;103(1):134–50.
830 76. Ververis A, Christodoulou A, Christoforou M, Kamilari C, Lederer CW, Santama N. A
831 novel family of katanin-like 2 protein isoforms (KATNAL2), interacting with nucleotide-
832 binding proteins Nubp1 and Nubp2, are key regulators of different MT-based processes in
833 mammalian cells. Cell Mol Life Sci. 2016;73(1):163–84.

77. Zhao X, Jin M, Wang M, Sun L, Hong X, Cao Y, Wang C. Fidgetin-like 1 is a ciliogenesis-inhibitory centrosome protein. Cell Cycle. 2016;15(17):2367–75.

78. Iwaya N, Akiyama K, Goda N, Tenno T, Fujiwara Y, Hamada D, Ikura T, Shirakawa M, Hiroaki H. Effect of Ca2+ on the microtubule-severing enzyme p60-katanin. Insight into the substrate-dependent activation mechanism. FEBS J. 2012;279(7):1339–52.

79. Buljan VA, Graeber MB, Holsinger RMD, Brown D, Hambly BD, Delikatny EJ, Vuletic VR, Krebs XN, Tomas IB, Bohorquez-Florez JJ, Liu GJ, Banati RB. Calcium–axonemal microtubuli interactions underlie mechanism(s) of primary cilia morphological changes. J Biol Phys. 2017;1–28.

80. Borghi N, Lowndes M, Maruthamuthu V, Gardel ML, Nelson WJ. Regulation of cell motile behavior by crosstalk between cadherin- and integrin-mediated adhesions. Proc Natl Acad Sci. 2010;107(30):13324–9.

863 **Figure 1. Serum stimulation of IMCD3 cells reveals non-canonical ciliary structures.**

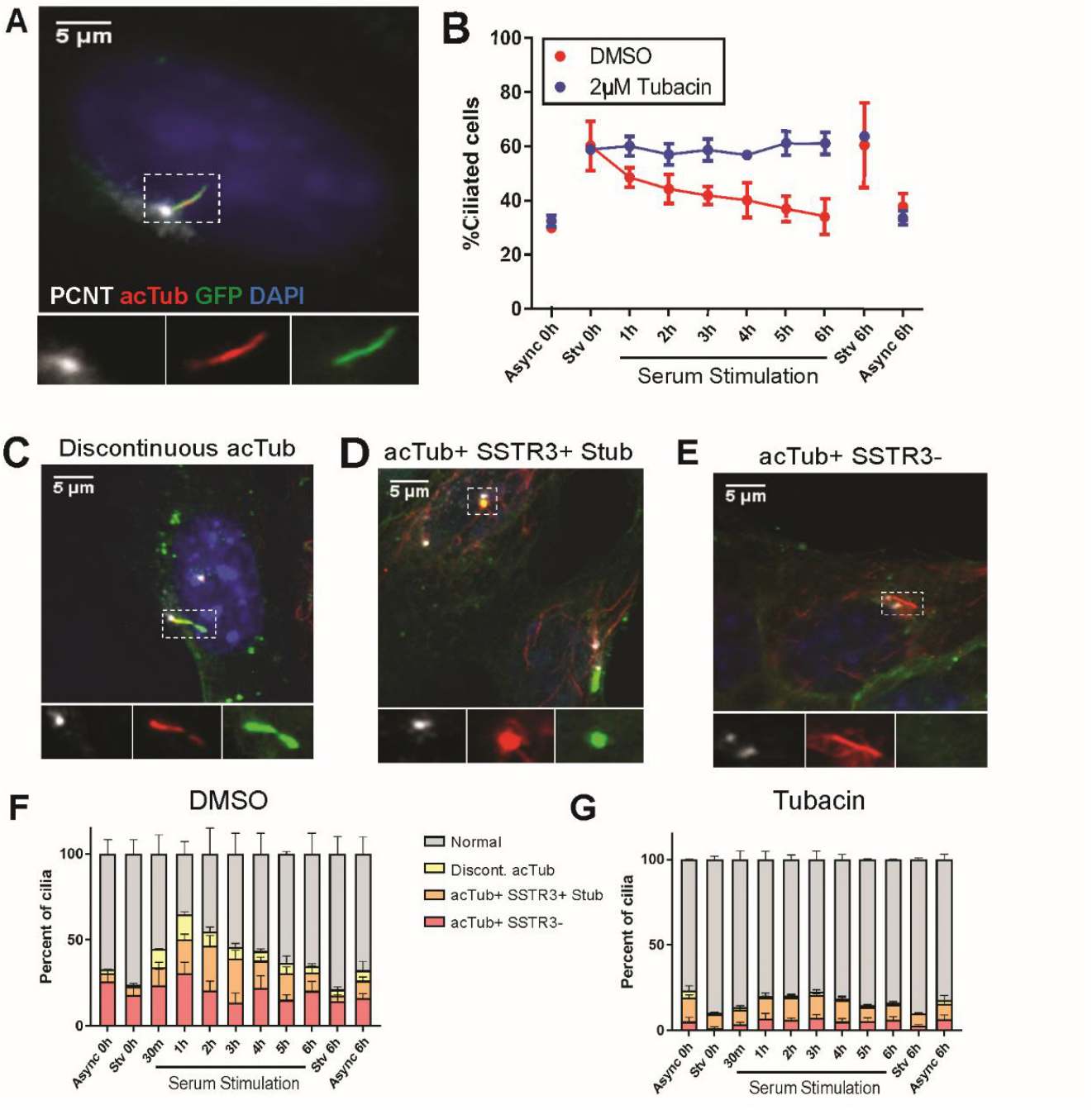

864

865

866

867

868

869

Figure S1. Characterization of immunostained serum stimulated cells.

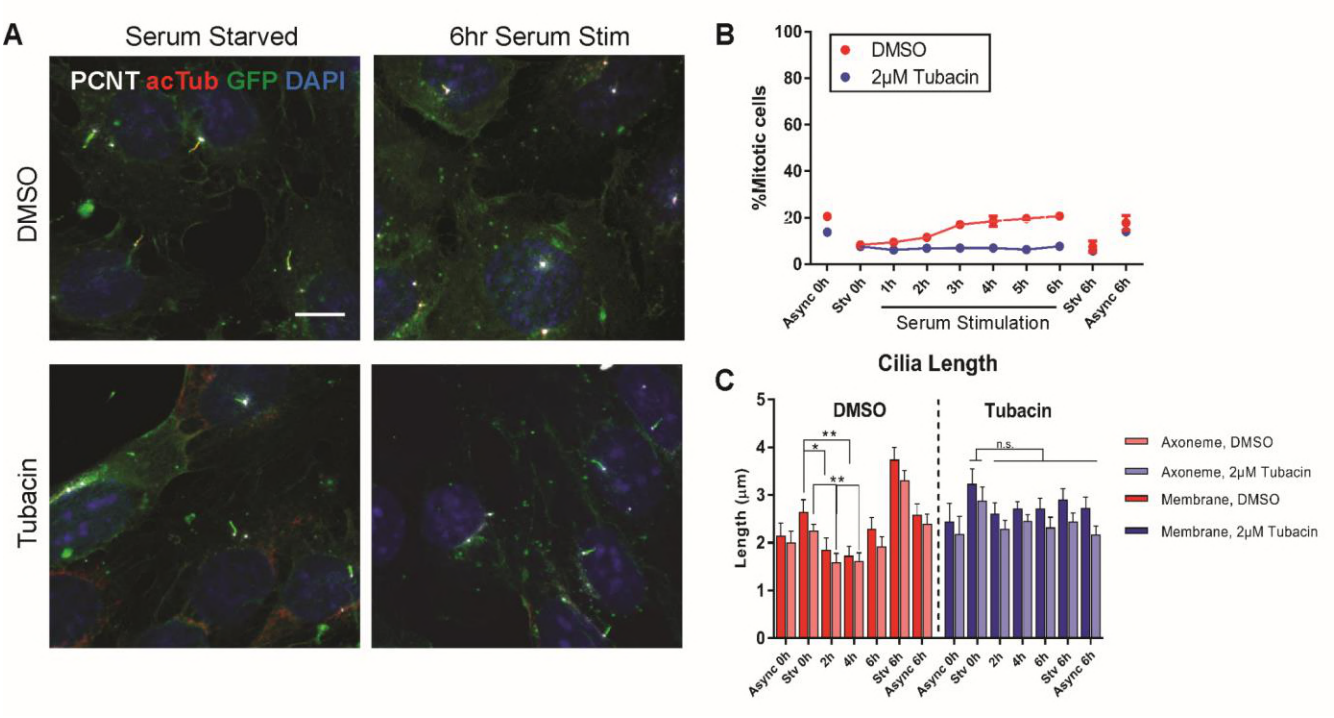

887 **Figure 2. Live-cell analysis of cilia disassembly reveal highly heterogeneous dynamics.**

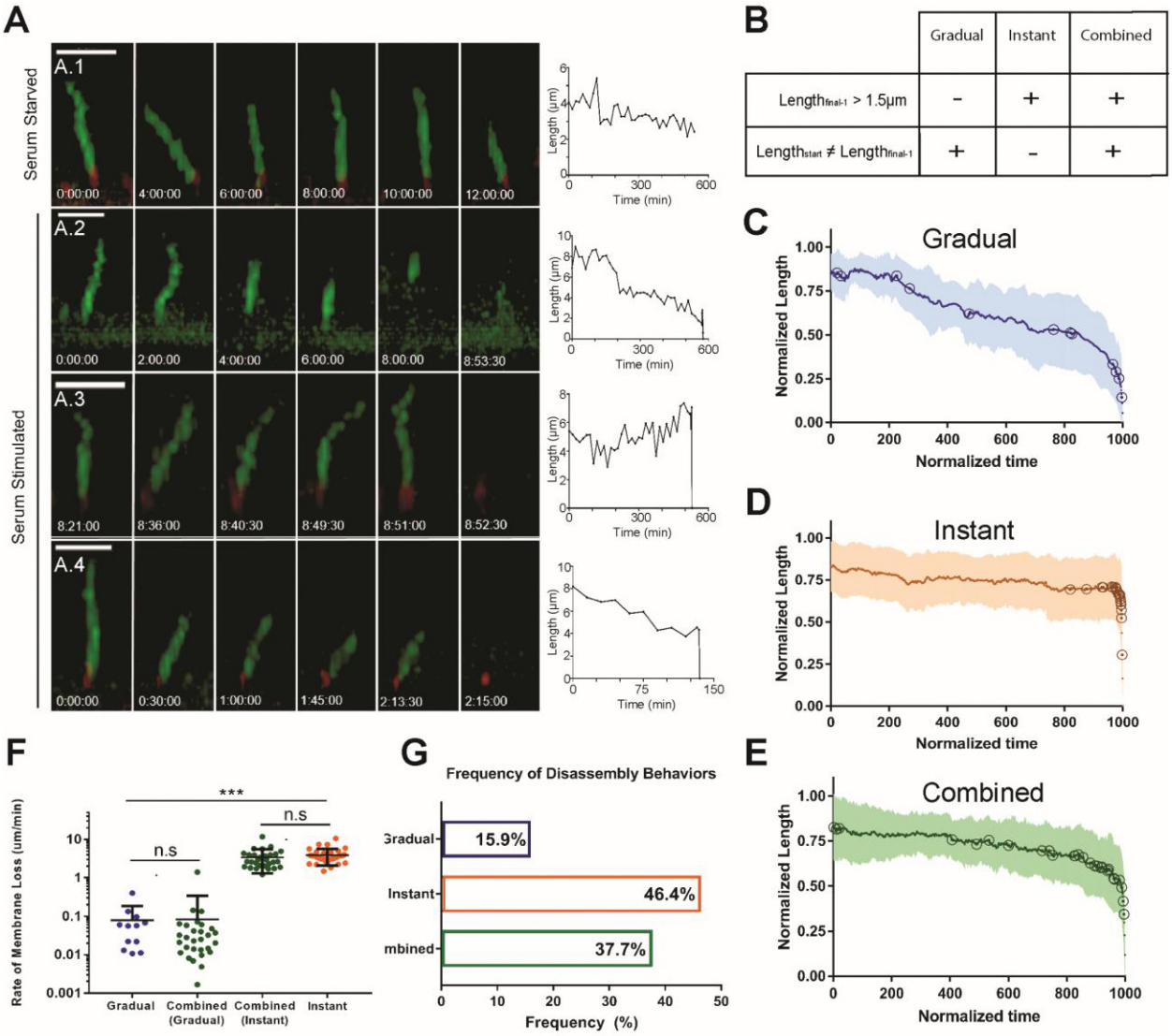

888

889

890

891

892

893

894

895

Figure S2. Manual analysis of ciliary disassembly dynamics.

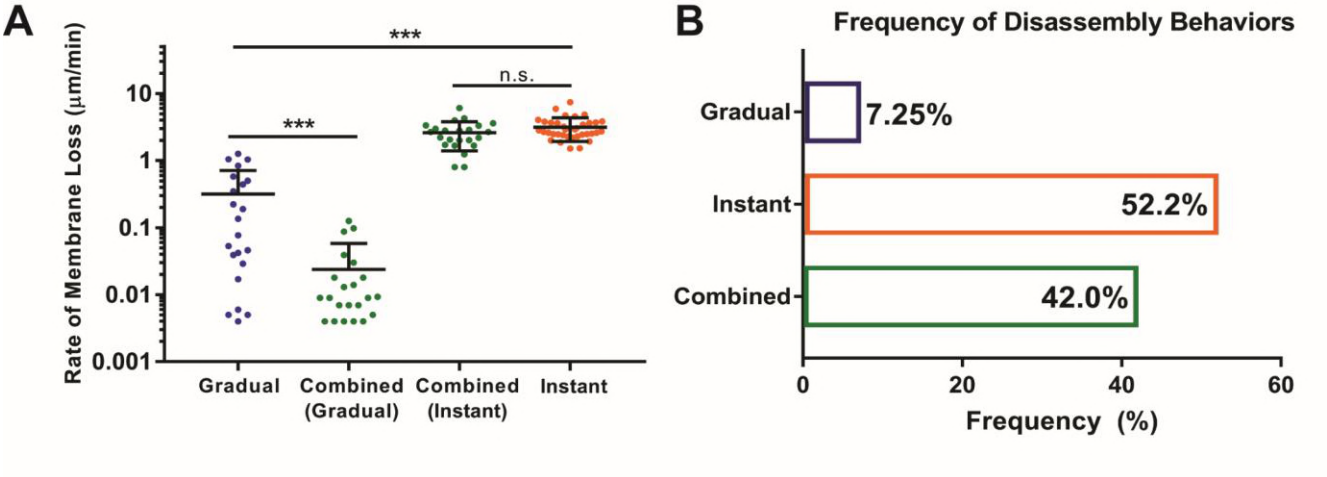

914 **Figure S3. Schematized workflow for automated analysis of ciliary disassembly dynamics.**

A

Analysis of serum starved control cilia (n=10)

	Length change over 12hr	% Change	Range (max-min)	Slope of best fit	Std. Dev.
Max	3.164	39%	9.193	-0.00103	1.532
Average	1.255	0.167%	6.466	-0.00463	1.116

B

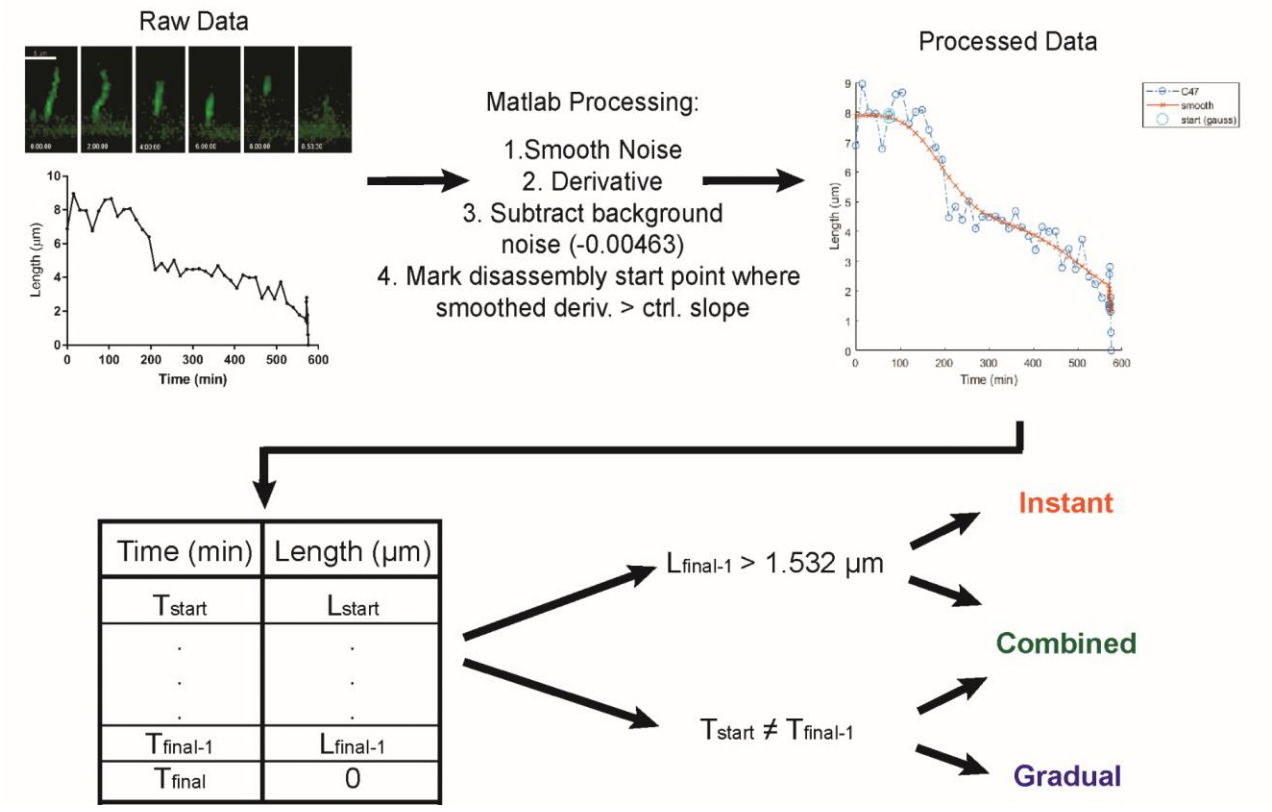

915

916

917

918

919

920

Figure S4. Timing of ciliary disassembly events.

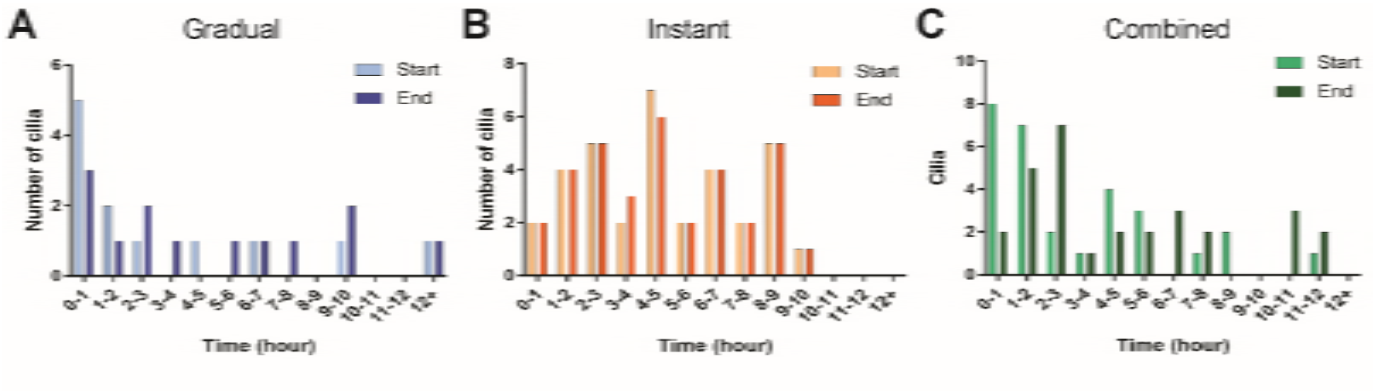

949 **Figure 3. Observation and validation of whole-cilium shedding.**
950

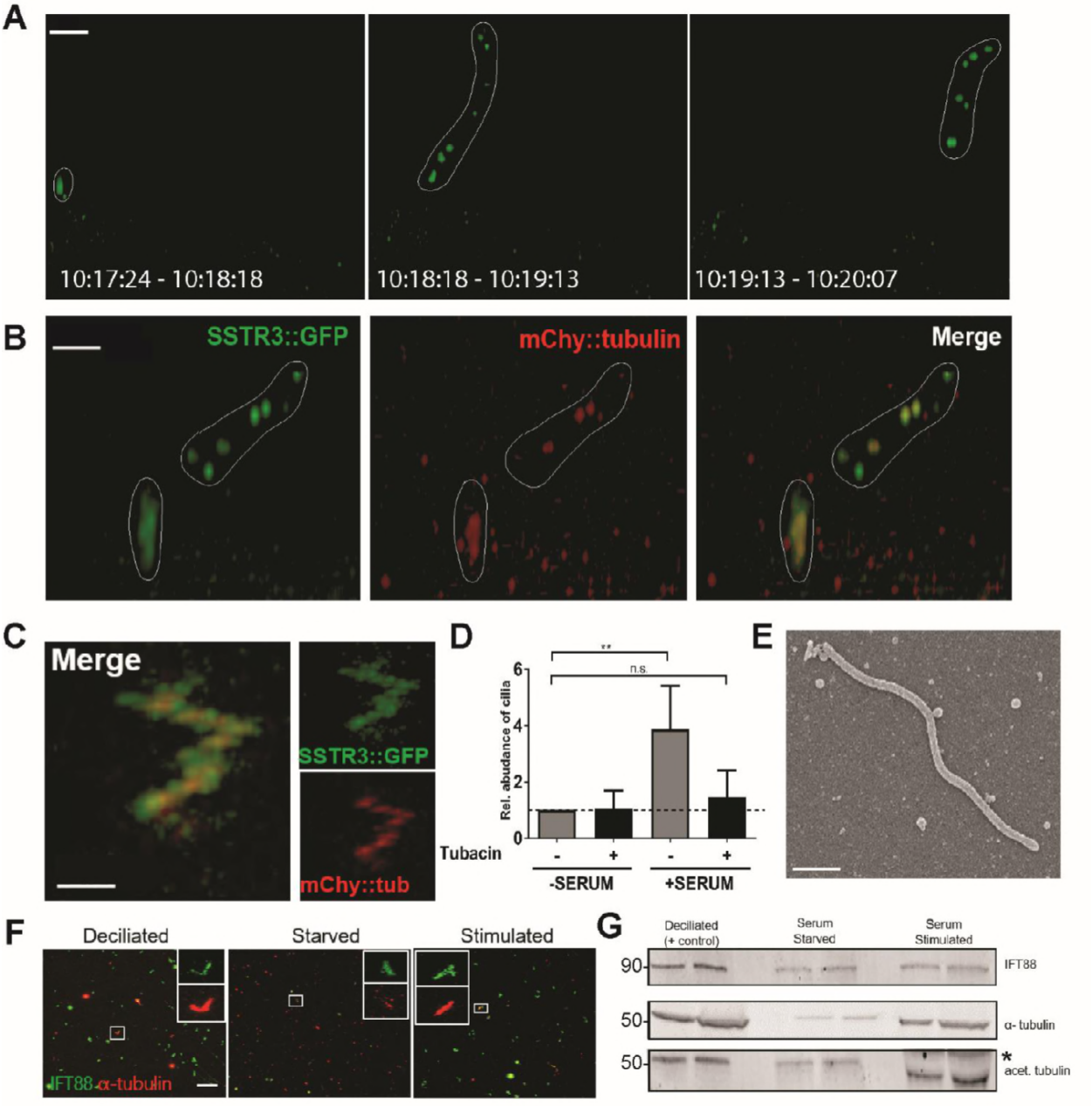

951
952
953
954
955
956
957
958
959

Figure S5. Dynamics of dibucaine-induced ciliary shedding are consistent with serum-induced *instant* disassembly.

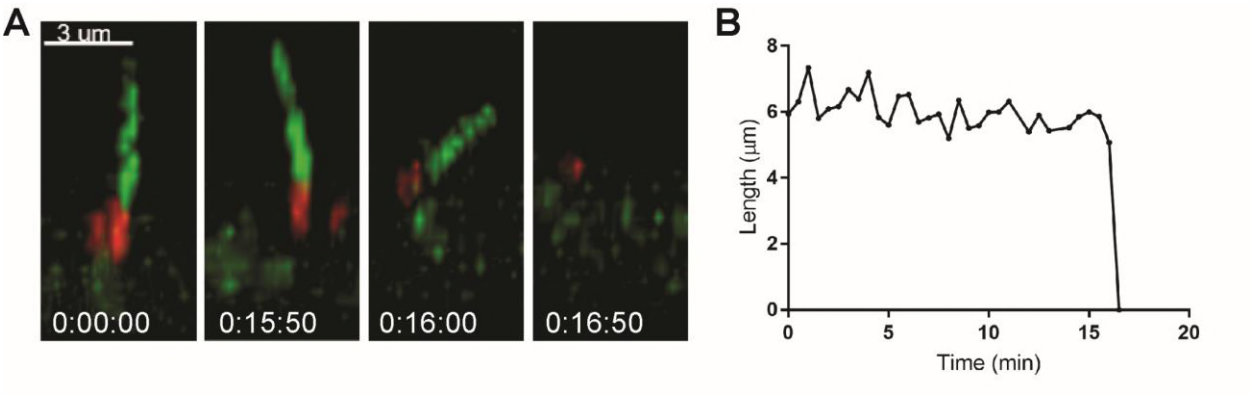

Figure S6. Schematics of cilia capture methods.

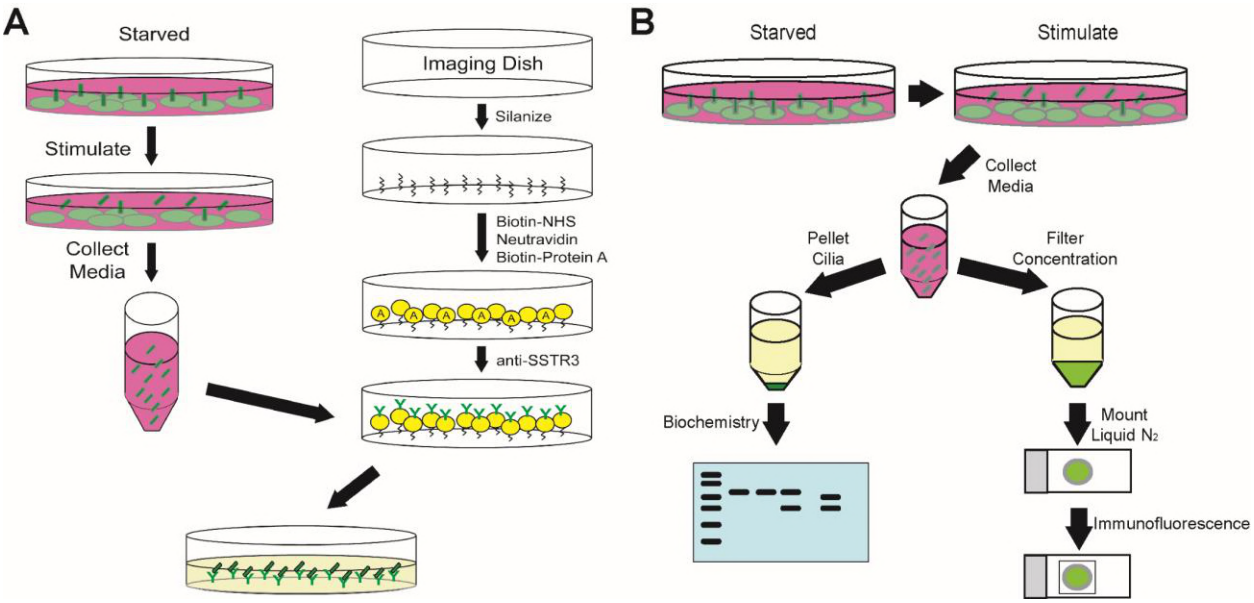

Figure 4. tRFP-p60 overexpression reduces ciliary length and promotes *instant* disassembly.

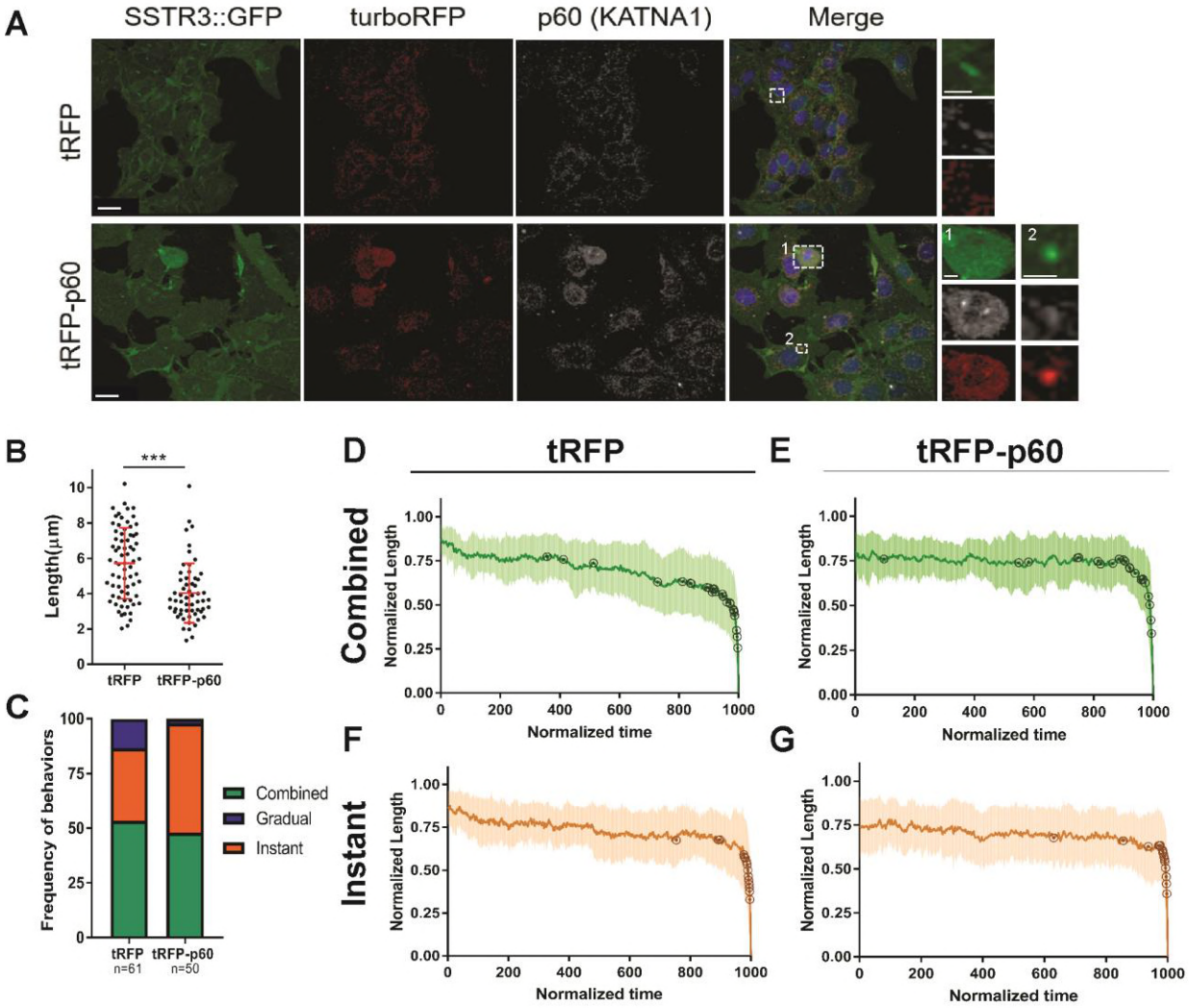

Figure S7. Characteriation of tRFP- and tRFP-p60 overexpressing IMCD3-SSTR3::GFP cells.

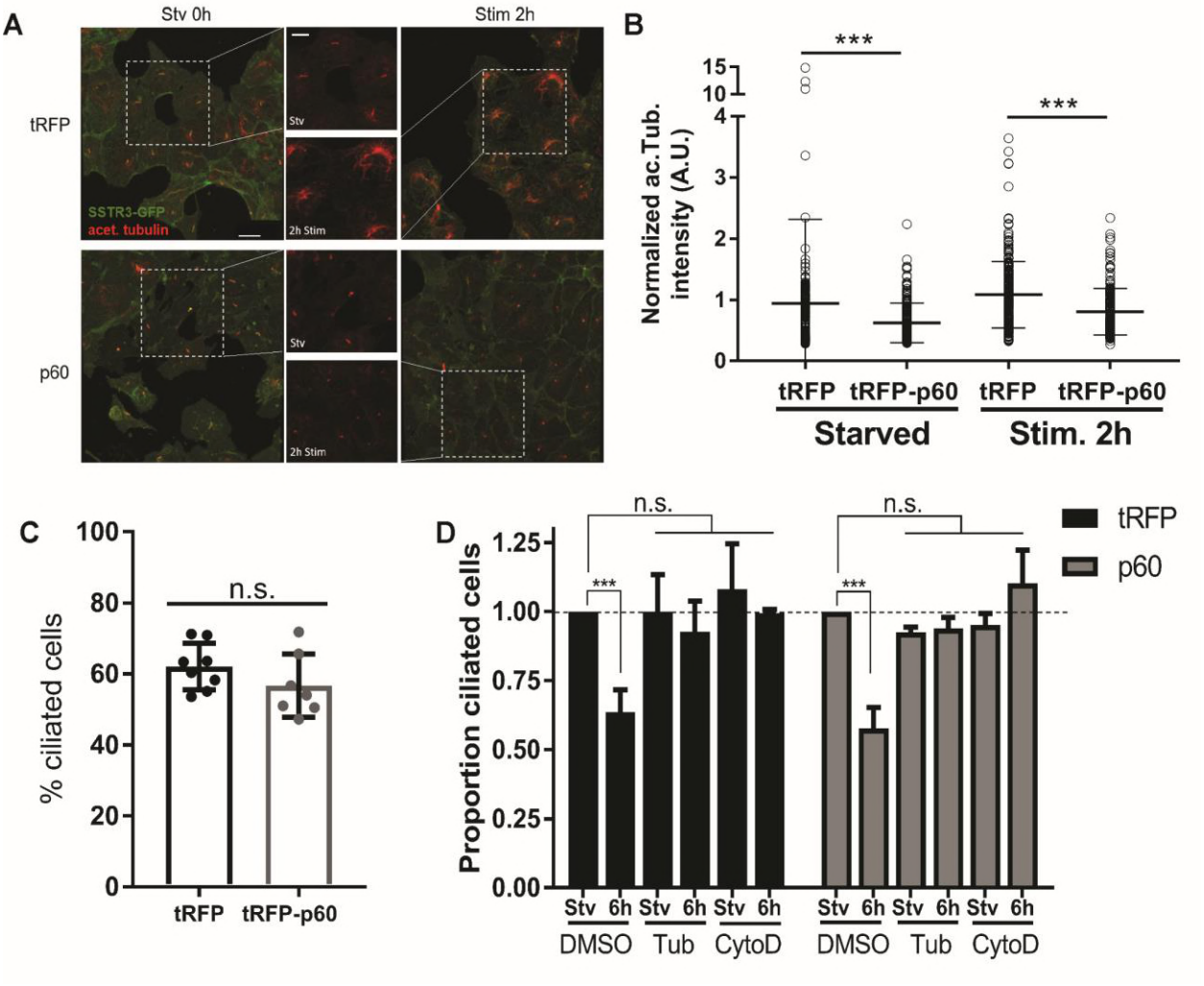

Figure 5. Effects of calcium-perturbing small molecules on ciliary abundance, length, and disassembly.

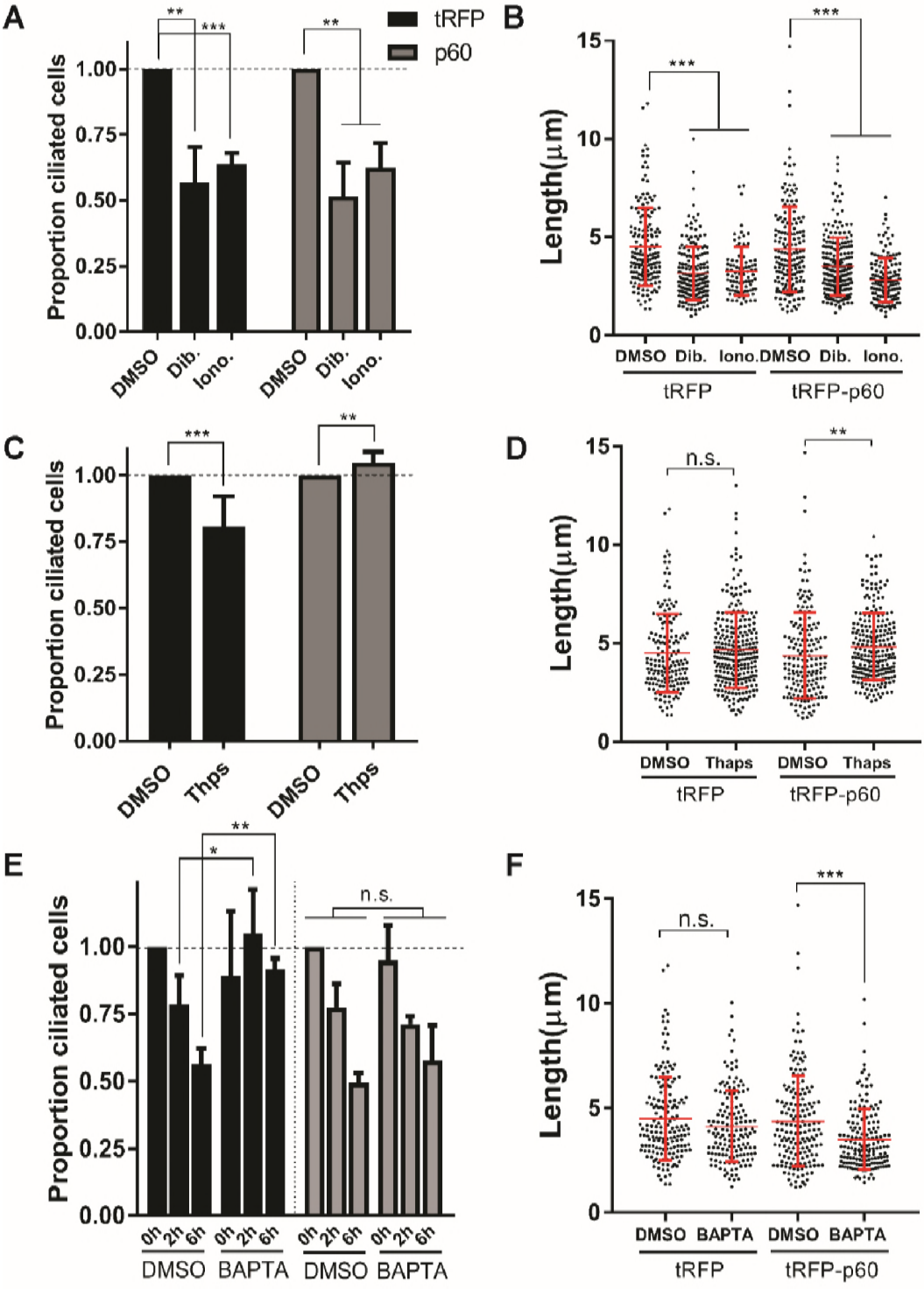

Figure Legends

Figure 1. Serum stimulation of IMCD3 cells reveals non-canonical ciliary structures. Serum starved IMCD3-SSTR3::GFP cells were stimulated with 10% serum in order to synchronize ciliary disassembly. A, C-E) Cells were fixed at indicated time points after serum addition and immunostained for pericentrin to mark the basal body (PCNT, white) and acetylated tubulin to mark the axoneme (acTub, red). A) Morphology of a normal, intact cilium in a starved cell. B) The population of ciliated cells quantified over a serum stimulation time course. Asynchronous (Async) and serum starved (Stv) controls were included at 0 hr and 6 hr. Cells treated in parallel with 2 μM tubacin. C-E) Non-canonical ciliary structures identified in serum stimulated cell populations. C) Discontinuous acTub staining, in this case accompanied by narrowing of the membrane. D) A ciliary stub, marked by punctate acTub and SSTR3 fluorescence. E) Full-length axoneme marked by acTub, lacking corresponding SSTR3::GFP signal. F-G) Stacked plots of cilia morphologies observed during serum stimulation in (F) DMSO and (G) tubacin-treated cells. Quantifications are based on means of 3 independent experiments with 150-200 cells analyzed per condition per replicate. Error bars – S.E.M. Statistical significance was assessed by unpaired t-test, *$p<0.05$, **$p<0.01$, ***$p<0.001$.

Figure S1. Characterization of immunostained serum stimulated cells. A) Serum starved and stimulated cells were immunostained for pericentrin to mark the basal body (PCNT, white) and acetylated tubulin to mark the axoneme (acTub, red). Scale bar, 10 μm. B) Serum stimulation is accompanied by an increase in mitotic cells, inhibited by tubacin treatment. C) Average ciliary length is decreased by in serum stimulated cells, but not in tubacin-treated cells. Length measurements were taken in FIJI for ciliary membrane (SSTR3-GFP) and axoneme (acetylated

tubulin). Quantifications are based on means of 3 independent experiments with 150-200 cells analyzed per condition per replicate. Error bars – S.E.M.

Figure 2. Live-cell analysis of cilia disassembly reveal highly heterogeneous dynamics. A) Still images and raw length curves representing dynamics of individual cilia disassembly events. Length measurements based on SSTR3::GFP fluorescence. Scale bar 5 μm. A.1) Control serum starved cilium measured over 12 hr period undergoes slight length change of 1.66 μm at a rate of 0.003 μm/min. A.2) Gradual disassembly with a rate of 0.016 μm/min. A.3) Instant disassembly, with an approximate minimum rate of 4.72 μm/min. A.4) Combined disassembly, consisting of an initial stage of gradual shortening at a rate of 0.029 μm/min, followed by instant loss at a minimum rate of 5.69 μm/min. B-E) Semi-automated analysis of disassembly events. B) Criteria for defining gradual, instant, and combined behaviors. Gradual: Length at next to last time point is significantly reduced from starting length. Instant: Length at next to last time point is above 1.5 μm threshold. Combined: both gradual and instant criteria are true. C-E) Cumulative normalized length vs. time curves for all (C) gradual, (D) instant, and (E) combined disassembly events. Open circles indicate individual event start points. F) Disassembly rates between dynamic groups vary by at least 2 orders of magnitude. Significance was determined by unpaired t-test, *$p<0.05$, **$p<0.01$, ***$p<0.001$. Error bars – S.D. H) Relative frequency of disassembly behaviors (n=70 from at least 10 independent experiments).

Figure S2. Manual analysis of ciliary disassembly dynamics. Raw length measurements were taken in Imaris and disassembly start points were judged by manual inspection. A) Rates of disassembly were calculated as change in length divided by duration of event. Statistical

1100 significance was determined by unpaired Student's t-test. B) Frequency of disassembly behaviors
1101 (n = 70 from at least 10 independent experiments).
1102
1103 *Figure S3. Schematized workflow for automated analysis of ciliary disassembly dynamics*. A) 10
1104 control non-disassembling cilia from starved cells were imaged at 90-sec intervals over a 12 hr
1105 period and analyzed. Cumulative metrics are shown here. Slight changes in length and stochastic
1106 length fluctuations are inherently present, and used as a baseline for analysis of disassembling
1107 cilia. Marked in yellow – maximum standard deviation of length is used as a proxy for length
1108 measurement error, and is thus used as a threshold length for instant disassembly; average slope
1109 of best fit line represents background decline in length over 12 hr imaging period. B) Matlab
1110 workflow. Scale bar, 5 μm. Raw data are run through a smoothing function. Derivatives are
1111 calculated, then normalized to background reduction (A) to identify start point of disassembly
1112 event. Lastly, disassembly behaviors (gradual, instant, and combined) are assigned as described in
1113 the text.
1114
1115 *Figure S4. Timing of ciliary disassembly events*. Histograms of A) gradual, B) instant, and C)
1116 combined disassembly events show frequency of disassembly start (light bars) and end (dark bars)
1117 points, binned by time post-serum stimulation.
1118
1119 *Figure 3. Observation and validation of whole-cilium shedding.* A) Serum stimulated cell, imaged
1120 at 54-second intervals. A short ciliary membrane is visibly shed from the cell surface. Shed cilium
1121 (in white outline) appears as a group of punctate fragments co-migrating due to high velocity of
1122 motion compared to speed of stack acquisition. Scale bar, 5 μm. B) Partial ciliary shedding in

IMCD3-SSTR3::GFP cells transiently expressing mCherry-α-tubulin, imaged at 30 s-intervals. Intact and shed portions of the cilium are demarcated with a white outline. Tubulin is visible in shed fragments. Scale bar, 3 μm. C-E) Ciliary immune-capture. Serum stimulation media were incubated on immobilized anti-SSTR3 antibody. Isolated cilia were observed by C-D) confocal fluorescent microscopy (scale bar, 2 μm) and E) SEM. Scale bar, 500nm. C-D) Immune-captured cilium from IMCD3-SSTR3::GFP cells transfected with mCherry-α-tubulin. D) Normalized quantification of (C), defined as elongated SSTR3+ objects at least 1.5 μm in length. Tubacin treatment reduces the prevalence of captured cilia. F-G) Filter-spin concentration of shed cilia. Serum stimulation media from IMCD3 cells with no endogenous fluorescence was concentrated either by (F) vacuum & centrifugation filtration for immunofluorescence or (G) centrifugation pelleting for subsequent Western blot. Media from artificially deciliated cells were included as a positive control. F) Filtration-concentrated samples were processed for immunofluorescence against IFT88 and α-tubulin. Scale bar, 20 μm. Representative insets show full-length cilia: 6.82μm (deciliated), 5.94μm (starved), and 6.10μm (stimulated). G) Western blot of concentrated material shows presence of ciliary markers at expected molecular weights: α-tubulin & acetylated tubulin. Molecular weights are indicated (kDa). Asterisk (*) denotes position of a large BSA band present in samples derived from serum-containing medium. Two technical replicates per condition are shown as side-by-side bands.

Figure S5. Dynamics of dibucaine-induced ciliary shedding are consistent with serum-induced instant disassembly. Starved cells were treated with 190 μm dibucaine and imaged by confocal microscopy at 30 sec intervals. A) Still images from a representative ciliary shedding show

1145 complete ciliary loss in under 30 sec. B) Length measurements from A) show instant
1146 disassembly dynamics.
1147
1148 *Figure S6. Schematics of cilia capture methods*. A) Immune-capture of shed cilia. Medium from
1149 serum stimulated cells is incubated on an imaging dish bearing immobilized antibody against the
1150 SSTR3 membrane marker. B) Filter-spin concentration of shed cilia. Medium from serum-
1151 stimulated cells is concentrated either by centrifugation pelleting for subsequent Western blot or
1152 by vacuum & centrifugation filtration for immunofluorescence. Medium from cells subjected to
1153 artificial deciliation was included as a positive control.
1154
1155 *Figure 4. tRFP-p60 overexpression reduces ciliary length and promotes instant disassembly*.
1156 IMCD3-SSTR3::GFP cells stably expressing turboRFP (tRFP) alone or tRFP-p60 fusion. A)
1157 tRFP and p60 cells were starved, fixed, and stained with a polyclonal antibody against p60.
1158 tRFP-p60 and p60 antibody label spindle poles (inset 1) and cilia (inset 2) in some cells. Scale
1159 bars, 20 μm. Inset scale bars, 5 μm. B) Cilia lengths measured from confocal stacks of live cells.
1160 Data pooled from at least 3 independent experiments, at least 50 cilia measured per experiment.
1161 Statistical significance from Mann-Whitney U test. B-G) Live-cell cilia disassembly dynamics.
1162 B) Relative frequencies of gradual, instant, and combined dynamic behaviors in tRFP and tRFP-
1163 p60 cells. Number of events analyzed is shown for each condition, each from at least 4
1164 independent experiments. D-G) Normalized average combined and instant disassembly plots
1165 with S.D. Gradual disassembly was excluded due to low incidence. Normalized individual
1166 disassembly start points are overlaid (circled points).
1167

Figure S7. Characteriation of tRFP- and tRFP-p60 overexpressing IMCD3-SSTR3::GFP cells. A) Starved and 2 hr-stimulated tRFP and tRFP-p60 cells were fixed and stained for acetylated tubulin (red, center column). Scale bar, 20 μm. Insets show acTub channel alone. Inset scale bar, 10 μm. B) Quantification of A). Mean cellular acTub intensity was normalized to cellular tRFP intensity. Data pooled from 3 independent experiments, 80-100 cells per condition. Statistical significance from Mann-Whitney U test. C) Percent ciliation calculated from fixed starved tRFP and tRFP-p60 cells. Data from at least 7 independent experiments. D) Cells pre-treated with DMSO, 2 μM Tubacin, or 1μM CytoD were starved and stimulated (6 hr). Proportion of ciliated cells was calculated by normalizing to Starved + DMSO for each cell line (dotted line). N = 3 experiments.

Figure 5. Effects of calcium-perturbing small molecules on ciliary abundance, length, and disassembly. Cilia counts are from fixed populations and normalized to respective DMSO controls. Length measurements are from live cells. A-B) tRFP and p60 cells were starved and pre-treated with DMSO, Dib. – 190 μM dibucaine (30 min), Iono. – 1 μM ionomycin (30 min), C-D) Thps – 5 μM thapsigargin (1 hr), or E-F) 1 μM BAPTA-AM (30 min). E) BAPTA-AM treated cells were subjected to serum stimulation, fixed and analyzed at indicated points. Data from 3 independent experiments, at least 100 cells counted per condition. Statistical significance was determined by unpaired t-test.

Supplementary Videos.

Video S1. *Primary cilium of a serum starved cell*. Imaged at 90 second intervals over 12 hrs, 45fps. The cilium undergoes rapid length fluctuations and a slight overall reduction in length at 0.003 μm/min. See Fig. 2A.1.

Video S2. *Primary cilium disassembling by gradual dynamics*. Imaged at 90 second intervals, 45fps. Cilium disassembles with an overall rate of 0.016μm/min. See Fig. 2A.2.

Video S3. *Primary cilium disassembling by instant dynamics*. Imaged at 90 second intervals, 15fps. Cilium is lost in under 90 seconds, approximate minimum rate of 4.72μm/min. See Fig. 2A.3.

Video S4. *Primary cilium disassembling by combined dynamics*. Imaged at 46 second intervals, 25fps. Cilium undergoes gradual shortening (0.029μm/min), followed by instant loss (>5.69μm/min). See Fig. 2A.4.

Video S5. *Primary cilium shedding*. Imaged at 54 second intervals. Ciliary membrane is released from cell surface (27:12-29:00). See Fig. 3A.